Neuron

Article

Astrocytic Piezo1-mediated mechanotransduction determines adult neurogenesis and cognitive functions

Graphical abstract

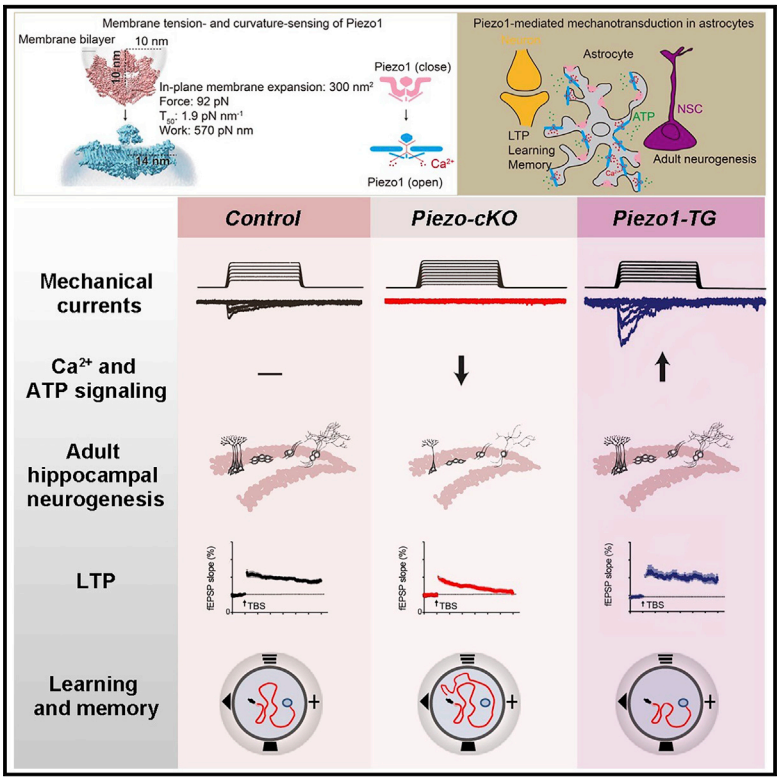

Highlights

- Piezo1 mediates mechanically evoked Ca^{2+} responses and ATP release in astrocytes
- Astrocytic deletion of Piezo reduces hippocampal volume and brain weight
- Astrocytic Piezo1 affects ATP-dependent adult neurogenesis *in vivo* and *in vitro*
- Astrocytic Piezo1 is necessary and sufficient in promoting LTP and learning and memory

Authors

Shaopeng Chi, Yaxiong Cui, Haiping Wang, ..., Zhuan Zhou, Yi Zhong, Bailong Xiao

Correspondence

xbailong@mail.tsinghua.edu.cn

In brief

Chi et al. find that astrocytes utilize the specialized mechanosensor Piezo1 to convert mechanical forces into Ca^{2+} and ATP signaling, which regulates adult neurogenesis and cognitive functions, conceptually highlighting the importance of mechanotransduction in brain structure and function.

Chi et al., 2022, Neuron *110*, 1–16
September 21, 2022 © 2022 Elsevier Inc.
https://doi.org/10.1016/j.neuron.2022.07.010

CellPress

Please cite this article in press as: Chi et al., Astrocytic Piezo1-mediated mechanotransduction determines adult neurogenesis and cognitive functions, Neuron (2022), https://doi.org/10.1016/j.neuron.2022.07.010

Neuron

CellPress

Article

Astrocytic Piezo1-mediated mechanotransduction determines adult neurogenesis and cognitive functions

Shaopeng Chi,[1,4] Yaxiong Cui,[1,4] Haiping Wang,[1,4] Jinghui Jiang,[1] Tingxin Zhang,[1] Suhua Sun,[2] Zhuan Zhou,[2] Yi Zhong,[3] and Bailong Xiao[1,5,*]

[1]State Key Laboratory of Membrane Biology, Tsinghua-Peking Center for Life Sciences, IDG/McGovern Institute for Brain Research, Beijing Frontier Research Center for Biological Structure, Beijing Advanced Innovation Center for Structural Biology, School of Pharmaceutical Sciences, Tsinghua University, Beijing 100084, China

[2]State Key Laboratory of Membrane Biology, Peking-Tsinghua Center for Life Sciences, PKU-IDG/McGovern Institute for Brain Research, College of Future Technology, Peking University, Beijing 100871, China

[3]Tsinghua-Peking Center for Life Sciences, IDG/McGovern Institute for Brain Research, School of Life Science, Tsinghua University, Beijing 100084, China

[4]These authors contributed equally

[5]Lead contact

*Correspondence: xbailong@mail.tsinghua.edu.cn

https://doi.org/10.1016/j.neuron.2022.07.010

SUMMARY

Adult brain activities are generally believed to be dominated by chemical and electrical transduction mechanisms. However, the importance of mechanotransduction mediated by mechano-gated ion channels in brain functions is less appreciated. Here, we show that the mechano-gated Piezo1 channel is expressed in the exploratory processes of astrocytes and utilizes its mechanosensitivity to mediate mechanically evoked Ca^{2+} responses and ATP release, establishing Piezo1-mediated mechano-chemo transduction in astrocytes. Piezo1 deletion in astrocytes causes a striking reduction of hippocampal volume and brain weight and severely impaired (but ATP-rescuable) adult neurogenesis *in vivo*, and it abolishes ATP-dependent potentiation of neural stem cell (NSC) proliferation *in vitro*. Piezo1-deficient mice show impaired hippocampal long-term potentiation (LTP) and learning and memory behaviors. By contrast, overexpression of Piezo1 in astrocytes sufficiently enhances mechanotransduction, LTP, and learning and memory performance. Thus, astrocytes utilize Piezo1-mediated mechanotransduction mechanisms to robustly regulate adult neurogenesis and cognitive functions, conceptually highlighting the importance of mechanotransduction in brain structure and function.

INTRODUCTION

Adult brain activities such as hippocampal neurogenesis and cognitive behaviors are generally believed to be dominated by chemical and electrical transduction mechanisms mediated by chemical receptors, ligand-gated and voltage-gated ion channels, respectively. By contrast, the involvement and importance of mechanotransduction mediated by mechano-gated ion channels in the central nervous system are relatively less appreciated. For instance, adult hippocampal neurogenesis is restricted in the specialized neurogenic niche of the subgranular zone (SGZ) of the hippocampal dentate gyrus (DG), where the maintenance, proliferation, and fate choices of neural stem cells (NSCs) are orchestrated by diverse cell types and local chemical and mechanical cues (Bond et al., 2015; Gonçalves et al., 2016). It has been well established that NSCs utilize diverse classes of signaling receptors to respond to a wide variety of chemical cues generated either by NSCs themselves or by other niche-constituting cell types such as astrocytes (Vicidomini et al., 2020). On the other hand, the cell types and molecular receptors that respond to the unique mechanical environment, composed of niche-residing cells, blood vessels, and extracellular matrix, remain substantially less understood (Vicidomini et al., 2020).

Astrocytes are morphologically complex cells that exist throughout the brain and mediate developmental, physiological, and pathological processes. For instance, astrocytes are a major type of hippocampal niche cells and promote proliferation and neuronal fate commitment of *in vitro* co-cultured NSCs, which might depend on secreted neurogenic factors (Song et al., 2002). However, the key niche cues that instruct hippocampal astrocytes to promote neurogenesis remain unclear. Astrocytes possess the characteristic morphology of abundant fine

Please cite this article in press as: Chi et al., Astrocytic Piezo1-mediated mechanotransduction determines adult neurogenesis and cognitive functions, Neuron (2022), https://doi.org/10.1016/j.neuron.2022.07.010

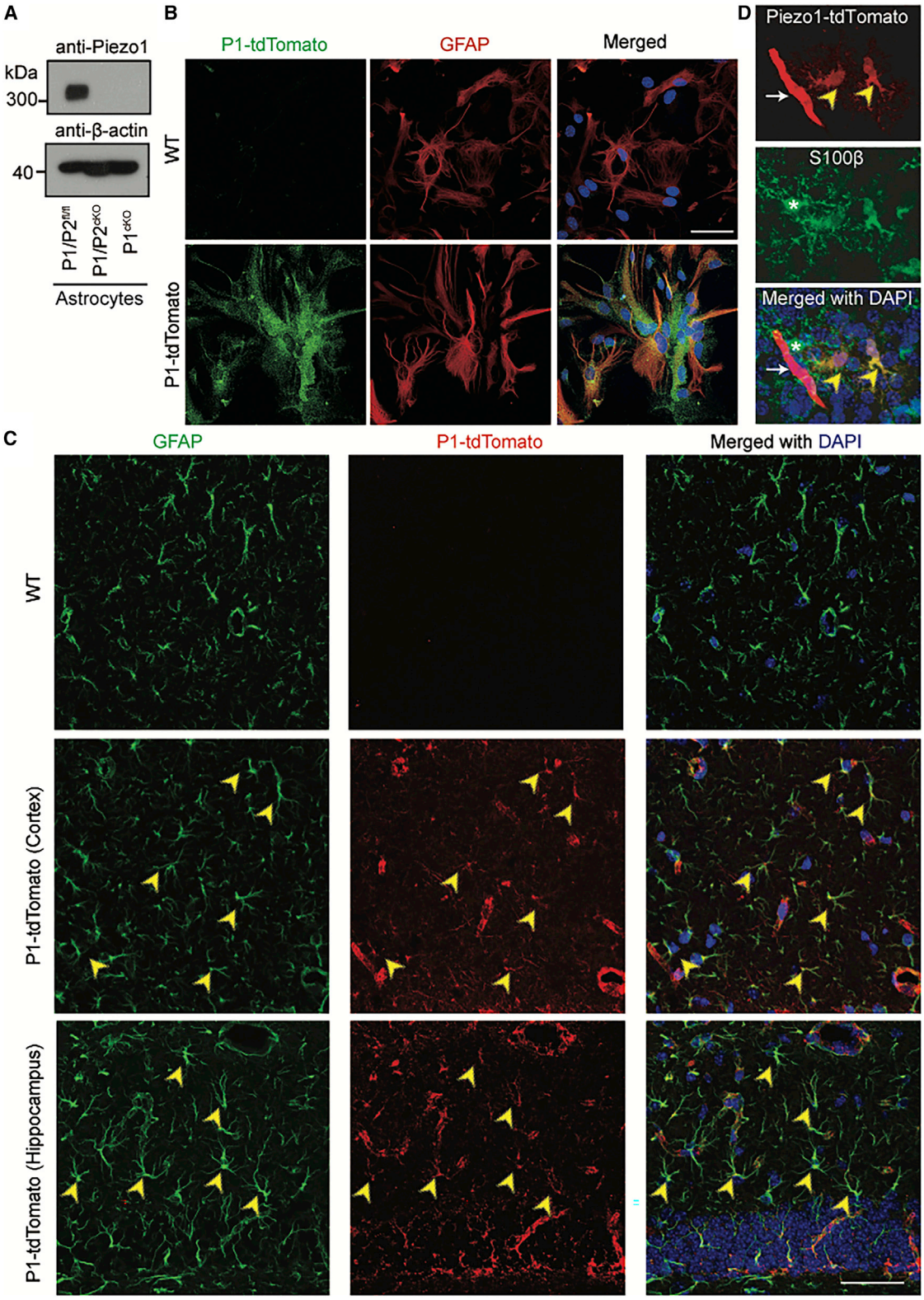

Figure 1. Expression of Piezo1 proteins in astrocytes

(A) Western blotting of Piezo1 from astrocyte lysates derived from the indicated mice.

(B) Immunostaining images of primarily cultured astrocytes derived from either the P1-tdTomato or wild-type (WT) mice. Scale bars, 50 μm.

(legend continued on next page)

processes that might allow them not only to explore the niche space but also to form direct interactions with other niche-constituting components, including NSCs themselves, blood vessels, and synapses of neurons (Vicidomini et al., 2020). Furthermore, astrocytes display spontaneously occurred, highly localized, and heterogeneous Ca^{2+} transients in their exploratory processes (Bindocci et al., 2017; Shigetomi et al., 2013a; Shigetomi et al., 2010), which are independent of neuronal spiking, metabotropic glutamate receptor activity, inositol trisphosphate (IP3) receptors, voltage-gated Ca^{2+} channels, TRPA1 channels, and store-operated Ca^{2+} release-activated Ca^{2+} (CRAC) channels (Rungta et al., 2016; Shigetomi et al., 2013b; Srinivasan et al., 2015; Toth et al., 2019). These observations indicate that non-uniformly distributed signals other than normally uniformly distributed chemical and electrical signals might be more relevant to activate the yet unidentified Ca^{2+}-permeable ion channels responsible for the spontaneous Ca^{2+} transients. In addition to responding to chemical signals, astrocytes show mechanosensitive cationic currents, Ca^{2+} responses, and ATP release upon mechanical stimulation (Bowman et al., 1992; Charles et al., 1991; Guthrie et al., 1999; Koizumi et al., 2003; Xiong et al., 2018), but the responsible mechano-gated cation channel remained unknown.

The groundbreaking discovery and establishment of the *bona fide* mechano-gated Piezo channel family, including Piezo1 and Piezo2 in mammals (Coste et al., 2010; Coste et al., 2012; Ge et al., 2015), have tremendously advanced our understanding of the physiological importance and molecular principles of mammalian mechanotransduction mechanisms (Douguet and Honoré, 2019). Given that no endogenous chemicals or physical stimuli other than mechanical force have been firmly established to activate Piezo1 or Piezo2, Piezos are considered as fully specialized mechanosensors for mediating versatile mechanotransduction in a wide variety of cell types (Jiang et al., 2021). Therefore, we hypothesize here that astrocytes might utilize Piezo channels as designated mechanosensors to explore the brain mechanical environment and consequently regulate adult brain activities such as hippocampal neurogenesis and cognitive behaviors.

RESULTS

Piezo1 proteins are expressed in astrocytes

Although previous studies have indicated the expression of Piezo1 in cultured astrocytes (Velasco-Estevez et al., 2020), its endogenous expression in brain tissues, mechanotransduction function, and *in vivo* physiological relevance have not been demonstrated using mouse genetics. Analysis of a single-cell RNA-seq dataset reveals detectable mRNA expression of Piezo1 in mouse brain astrocytes, comparable to that of the ATP release channel pannexin1 (Figures S1A and S1B) (Zeisel et al., 2018). By contrast, other ion channels potentially involved in astrocyte mechanotransduction and Ca^{2+} signaling, including Piezo2, TRPV4, and TRPA1, are much less frequently detected, whereas the gap junction channel connexin43 and the astrocyte marker gene glial fibrillary acidic protein (GFAP) show high expression (Figure S1A). RT-PCR confirmed Piezo1 expression in cultured cortical astrocytes, whereas cortical neurons had a much lower expression (Figure S1C).

To assay the expression and functional role of Piezo channels in astrocytes, we generated mice containing both the floxed Piezo1 and Piezo2 genes (P1/P2$^{fl/fl}$, defined as control mice [Ctrl] in the text and figures) and employed the commonly used human glial fibrillary acidic protein (hGFAP)-Cre line (Zhuo et al., 2001) to delete them together from astrocytes, generating the GFAP-Cre;P1/P2$^{fl/fl}$ mice (defined as cKO). cKO astrocytes had significantly reduced mRNA expression of Piezo1 (Figure S1C). Western blotting detected Piezo1 proteins in astrocyte lysates derived from the Ctrl mice, but not from the littermate cKO mice or the Piezo1 alone-deficient mice (GFAP-Cre; Piezo1$^{fl/fl}$, Piezo1^{cKO}) (Figures 1A and S1D). Consistent with the single-cell RNA-seq analysis (Figure S1A), Piezo2 was not detected in astrocytes despite its successful detection in lysates derived from dorsal root ganglia (DRG) neurons, where Piezo2 is known to be expressed for mediating somatosensation of mechanical stimuli (Ranade et al., 2014b) (Figure S1D).

We next examined the expression and subcellular localization of Piezo1 in astrocytes. Due to the lack of Piezo1 antibodies that are suitable for specifically immunostaining endogenously expressed Piezo1, we used the previously reported Piezo1-tdTomato knockin mouse line (Piezo1-tdTomato-KI) (Ranade et al., 2014a). Anti-dsRed antibody immunostaining revealed Piezo1-tdTomato protein expression specifically in primarily cultured astrocytes derived from the Piezo1-tdTomato-KI mice, but not from the wild-type Ctrl mice (Figure 1B). The cellular distribution of Piezo1-tdTomato proteins on both the peripheral plasma membrane and intracellular membrane in astrocytes is consistent with those observed in other cell types such as macrophage, keratinocyte, and fibroblast (Ellefsen et al., 2019; Holt et al., 2021; Ma et al., 2021). Importantly, *in vivo* Piezo1-tdTomato expression was detected in both cortical and hippocampal astrocytes in brain slices derived from the Piezo1-tdTomato-KI mice, albeit with varied expression levels among astrocytes (Figures 1C and 1D). Piezo1-tdTomato proteins were located in both the soma and processes of astrocytes (Figure 1D). Consistent with high expression of Piezo1 in endothelial cells of peripheral blood vessels (Ranade et al., 2014a), brain blood vessels had strong Piezo1-tdTomato expression as well (Figure 1D).

Piezo1 mediates mechanically evoked cationic currents and Ca^{2+} signaling in astrocytes

To examine whether Piezo1 might directly mediate mechanically activated (MA) cationic currents (Bowman et al., 1992), we first

(C) Immunostaining of Piezo1-tdTomato and the astrocyte marker GFAP from brain slice derived from either WT or the Piezo1-tdTomato-KI mice. DAPI was used for staining the nucleus. Scale bars, 50 μm. Yellow arrow heads indicate astrocytes co-expressing GFAP and Piezo1-tdTomato.

(D) Immunostaining of Piezo1-tdTomato and the astrocyte marker S100ß from brain slice derived from the Piezo1-tdTomato-KI mice. DAPI was used for staining the nucleus. Scale bars, 20 μm. Yellow arrow heads indicate astrocytes with relatively high expression of Piezo1-tdTomato in both somas and processes, while the white star indicates the astrocyte with low expression. The white arrow indicates blood vessels showing high expression of Piezo1-tdTomato.

Please cite this article in press as: Chi et al., Astrocytic Piezo1-mediated mechanotransduction determines adult neurogenesis and cognitive functions, Neuron (2022), https://doi.org/10.1016/j.neuron.2022.07.010

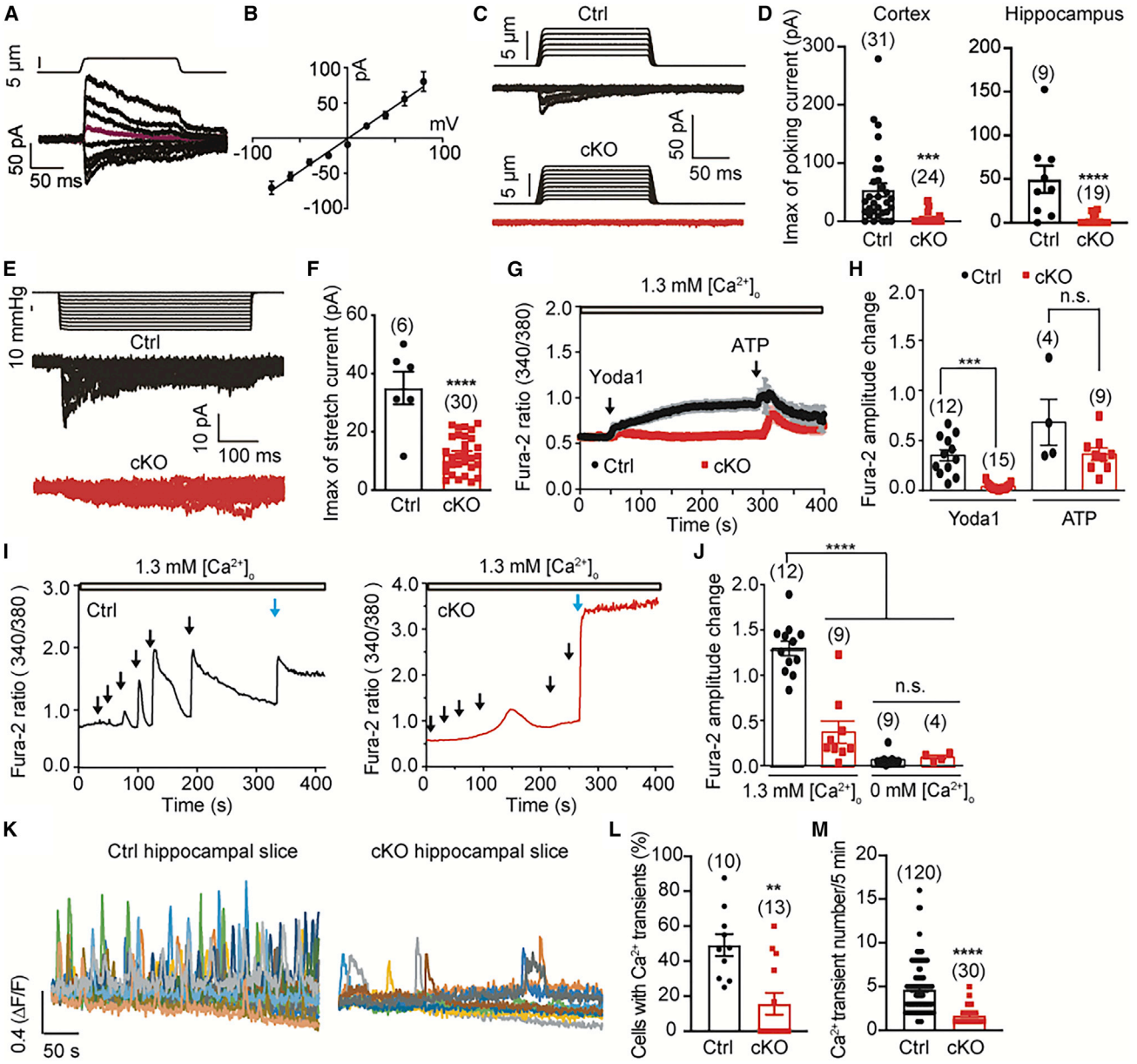

Figure 2. Piezo1 mediates mechanically evoked cationic currents and Ca^{2+} influx in astrocytes

(A) Representative whole-cell currents of astrocytes in response to the poking step under varying holding voltages. The purple trace indicates recording at +20 mV.

(B) Linear plot of the current-voltage relationship.

(C) Representative whole-cell currents of the indicated astrocytes in response to the poking steps at a holding voltage of −60 mV.

(D) Scatterplot of maximal MA currents of astrocytes derived from either cortex or hippocampus. Each bar represents mean ± SEM, and the recorded cell number is labeled above the bar. Unpaired Student's t test. ***$p < 0.001$, ****$p < 0.0001$.

(E) Representative stretch-induced currents of the indicated astrocytes in response to the indicated negative pressures at a holding voltage of −80 mV.

(F) Scatterplot of maximal stretch-induced currents. Each bar represents mean ± SEM, and the recorded cell number is labeled above the bar. Unpaired Student's t test. ***$p < 0.001$.

(G) Representative single-cell fura-2 Ca^{2+} imaging of astrocytes derived from either the Ctrl or cKO mice in response to Yoda1 and ATP.

(H) Scatterplot of fura-2 amplitude changes in response to Yoda1 and ATP. Each bar represents mean ± SEM, and the number of imaged coverslips is labeled above the bar. Unpaired Student's t test.***$p < 0.001$. n.s. represents non-significance.

(I) Representative single-cell fura-2 Ca^{2+} imaging traces of the indicated astrocytes in response to increased poking stimulation indicated by the arrows. The last arrow in cyan indicates the irreversible fura-2 signal change due to rupture of the cell.

(legend continued on next page)

Please cite this article in press as: Chi et al., Astrocytic Piezo1-mediated mechanotransduction determines adult neurogenesis and cognitive functions, Neuron (2022), https://doi.org/10.1016/j.neuron.2022.07.010

carried out whole-cell electrophysiological recordings from primarily cultured astrocytes while simultaneously indenting the cell membrane with a piezo-driven blunt glass pipette, which is a standard assay for measuring Piezo-mediated MA currents. In astrocytes derived from the Ctrl mice, we recorded MA currents showing a linear current-voltage relationship with a reversal potential of 1.7 ± 2.7 mV, poking-step dependence, and an inactivation at the holding potential of −60 mV, which support the existence of non-selective cationic currents in astrocytes (Figures 2A–2C). Importantly, the current was nearly abolished in both cortical and hippocampal astrocytes derived from the cKO mice (Figures 2C and 2D) or from the Piezo1^{cKO} mice (Figures S2A and S2B). Furthermore, we observed stretch-dependent inward currents from the Ctrl astrocytes, which were drastically reduced in the cKO cells (Figures 2E and 2F). In contrast to the expression and function of Piezo1 in astrocytes, no Piezo1 was detected in NSCs derived from the P1/P2$^{fl/fl}$ Ctrl mice infected with retrovirus encoding either EGFP or EGFP-2A-Cre (Figure S2C). Furthermore, primarily cultured NSCs or hippocampal and cortical neurons did not show Piezo-dependent poking-induced currents (Figures S2D–S2F). The lack of functional expression of Piezo channels in NSCs and neurons excludes the potential complication of GFAP-Cre-mediated deletion of Piezo1 and Piezo2 from NSCs and neurons in the cKO mice. Taken together, the expression and electrophysiological characterizations demonstrate that Piezo1, but not Piezo2, is located in the plasma membrane to mediate MA cationic currents in astrocytes. To avoid any potential Piezo2-mediated compensation upon Piezo1 deletion, we mainly used the P1/P2$^{fl/fl}$ (Ctrl) and GFAP-Cre;P1/P2$^{fl/fl}$ (cKO) littermate mice in subsequent studies.

Astrocyte Ca^{2+} signaling includes both intracellular Ca^{2+} release from endoplasmic reticulum (ER) in the soma and frequently occurred and localized Ca^{2+} influx in the processes (Bazargani and Attwell, 2016). While it is well established that the Ca^{2+} release is mediated by IP3 receptors (Fiacco et al., 2007), the Ca^{2+}-permeable ion channel mediating localized Ca^{2+} influx in astrocytes is unclear (Bazargani and Attwell, 2016; Srinivasan et al., 2015). To examine whether Piezo1 might mediate Ca^{2+} influx in astrocytes, we first carried out single-cell Ca^{2+} imaging of fura-2, a ratiometric Ca^{2+} dye, in primarily cultured astrocytes derived from either the Ctrl or cKO mice. Yoda1, a Piezo1 chemical activator (Syeda et al., 2015), consistently increased the fura-2 signal in the Ctrl astrocytes, but not in the cKO cells (Figures 2G and 2H). Furthermore, the Yoda1 response was completely abolished by removing extracellular Ca^{2+} (Figure S2G), demonstrating that Piezo1 mediates Yoda1-induced Ca^{2+} influx rather than Ca^{2+} release from the ER Ca^{2+} store. Both the Ctrl and cKO cells responded similarly to ATP or glutamate, which are glial transmitters and induce Ca^{2+} release from ER, suggesting that the cKO cells retain normal responses to glial transmitter-induced Ca^{2+} signaling (Figures 2G, 2H, and S2H).

To examine whether Piezo1 might mediate mechanically evoked Ca^{2+} responses in astrocytes, we carried out single-cell Ca^{2+} imaging of astrocytes while simultaneously indenting the cell membrane using a piezo-driven blunt glass pipette, which was originally used to discover the mechanical responses of astrocytes. Interestingly, the Ctrl astrocytes showed reversible Ca^{2+} increase in a poking displacement-dependent manner (Figure 2I). Increasing the probe displacement resulted in larger and more sustained enhancement of the fura-2 signal until the ultimate occurrence of an irreversible change (Figure 2I, indicated by the cyan arrow), which we considered as an indication of membrane rupture and cell damage. Importantly, poking-induced reversible change of fura-2 signal was much less frequently observed in the cKO astrocytes (Figure 2I). The fura-2 amplitude change induced by the maximal poking displacement prior to cell damage was also significantly reduced in the cKO astrocytes (Figures 2I and 2J). In both the Ctrl and cKO cells, removing extracellular Ca^{2+} totally abolished poking-induced responses (Figures 2J and S2I). Together, these data demonstrate that Piezo1 mediates MA Ca^{2+} influx in astrocytes, in line with its role in mediating the MA cationic currents.

To test whether Piezo1 might mediate Ca^{2+} transients in native astrocytes in the absence of externally applied mechanical force, we carried out two-photon Ca^{2+} imaging of hippocampal slices, which were loaded with the Ca^{2+} dye fluo-4 and the astrocyte-specific dye sulforhodmine 101 (SR101). Consistent with previous reports (Rungta et al., 2016), we detected frequently occurred Ca^{2+} transients in SR101-positive astrocytes derived from the Ctrl mice (Figure 2K). Importantly, such responses were drastically reduced in the cKO astrocytes (Figure 2K). cKO slices showed significantly less astrocytes displaying Ca^{2+} transients than Ctrl slices (Figure 2L), and the Ca^{2+} transient frequency of cKO astrocytes was also much lower than that of Ctrl astrocytes (Figure 2M). By contrast, both the Ctrl and cKO slices had comparable ATP responses (Figures S2J and S2K), suggesting unaltered intracellular Ca^{2+} release in response to ATP stimulation. Collectively, these data suggest that Piezo1 plays a prominent role in mediating spontaneously occurred Ca^{2+} influx in astrocytes.

Piezo1 mediates mechanically evoked ATP release from astrocytes

Astrocyte Ca^{2+} signaling can trigger the release of gliotransmitters such as ATP (Araque et al., 2014; Newman, 2001;

(J) Scatterplot of maximal fura-2 amplitude changes in response to poking in the presence or absence of extracellular Ca^{2+}. The last poking-induced irreversible fura-2 change was excluded from analysis. Each bar represents mean ± SEM, and the number of analyzed coverslips is labeled above the bar. Unpaired Student's t test. ****$p < 0.0001$. n.s. represents non-significance.
(K) Representative fluo-4 Ca^{2+} transients of astrocytes derived from the indicated hippocampal slices using two-photon imaging. Each color trace represents the response of an individual astrocyte in the imaged slice. 15 and 9 astrocytes with Ca^{2+} transients are shown for the Ctrl and cKO hippocampal slices, respectively.
(L) Scatterplot of percentage of astrocytes showing Ca^{2+} transients from the indicated hippocampal slices. Each bar represents mean ± SEM, and the number of analyzed slices is labeled above the bar. Unpaired Student's t test. **$p < 0.01$.
(M) Scatterplot of the number of Ca^{2+} transients during a 5-min period from the indicated astrocytes showing Ca^{2+} transients. Each bar represents mean ± SEM, and the number of analyzed astrocytes is labeled above the bar. Unpaired Student's t test. ****$p < 0.0001$.

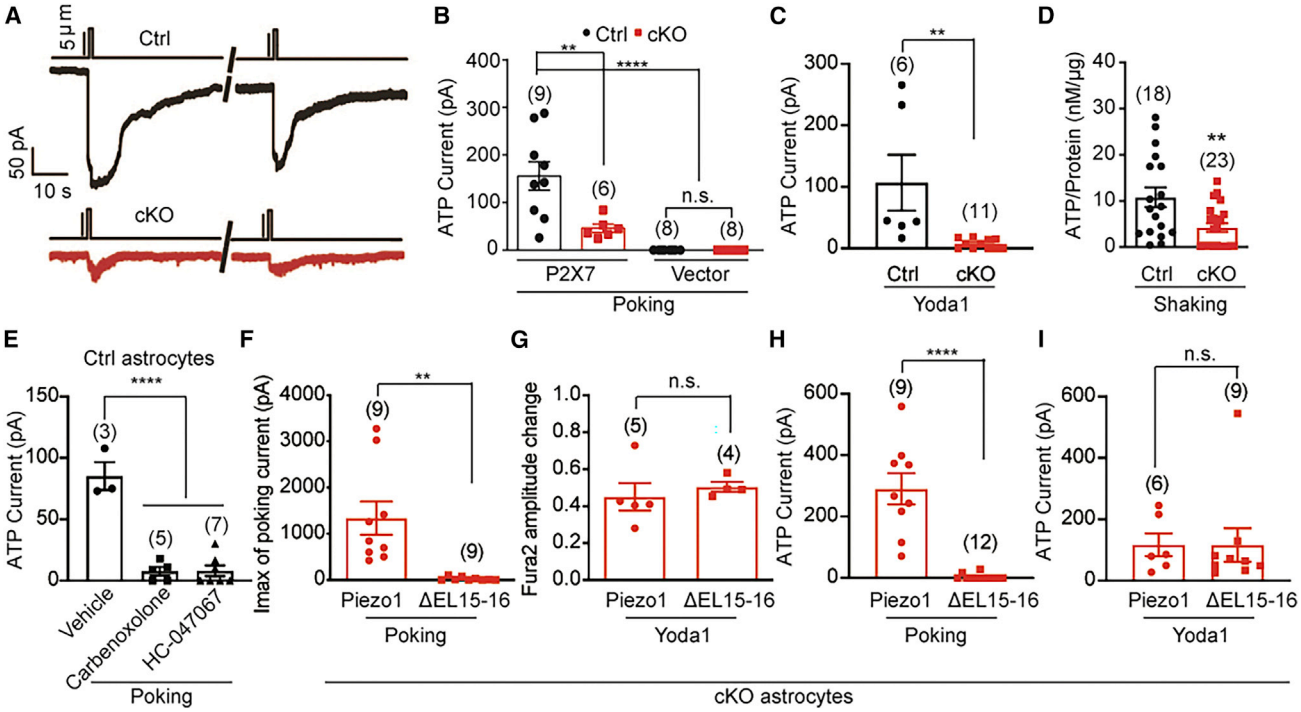

Figure 3. Piezo1 mechanosensitivity mediates mechanically evoked ATP release in astrocytes

(A) Representative whole-cell currents of the P2X7-expressing "sniffer" HEK293T cells (sniffer ATP current) in response to poking of the neighboring Ctrl or cKO astrocytes.

(B) Scatterplot of the currents recorded from the sniffer cells or the vector-transfected control cells in response to poking of the neighboring Ctrl or cKO astrocytes. Each bar represents mean ± SEM, and the recorded cell number is labeled above the bar. Unpaired Student's t test. ****$p < 0.0001$, **$p < 0.01$.

(C) Scatterplot of the sniffer ATP current in response to Yoda1-stimulated Ctrl or cKO astrocytes. Each bar represents mean ± SEM, and the recorded cell number is labeled above the bar. Unpaired Student's t test. **$p < 0.01$.

(D) Scatterplot of ATP concentration (normalized to the protein level of the lysed cells) measured from supernatant of the indicated astrocytes that were subjected to shaking. Each bar represents mean ± SEM, and the number of measurement is labeled above the bar. Unpaired Student's t test. **$p < 0.01$.

(E) Scatterplot of the sniffer ATP current in response to poking of the neighboring WT astrocytes in the presence of either 100 μM carbenoxolone for blocking connexin/pannexin channels or 10 μM HC-067047 for blocking TRPV4 channels. Each bar represents mean ± SEM, and the recorded cell number is labeled above the bar. Unpaired Student's t test. ****$p < 0.0001$.

(F) Scatterplot of maximal MA currents of cKO astrocytes transfected with either WT Piezo1 or the Piezo1-ΔEL15-16 mutant. Each bar represents mean ± SEM, and the recorded cell number is labeled above the bar. Unpaired Student's t test. ***$p < 0.001$.

(G) Scatterplot of fura-2 amplitude changes of cKO astrocytes transfected with either WT Piezo1 or the Piezo1-ΔEL15-16 mutant in response to Yoda1. Each bar represents mean ± SEM, and the number of imaged coverslips is labeled above the bar. Unpaired Student's t test. n.s. represents non-significance.

(H) Scatterplot of the sniffer ATP current in response to poking of the neighboring cKO astrocytes transfected with either WT Piezo1 or the Piezo1-ΔEL15-16 mutant. Each bar represents mean ± SEM, and the recorded cell number is labeled above the bar. Unpaired Student's t test. ****$p < 0.0001$.

(I) Scatterplot of the sniffer ATP current in response to Yoda1-stimulated cKO astrocytes transfected with either WT Piezo1 or the Piezo1-ΔEL15-16 mutant. Each bar represents mean ± SEM, and the recorded cell number is labeled above the bar. Unpaired Student's t test. n.s. represents non-significance.

Pryazhnikov and Khiroug, 2008). Previous studies have shown that mechanical stimulation induces ATP release from astrocytes (Koizumi et al., 2003; Newman, 2001). We therefore examined whether mechanical activation of Piezo1 might trigger ATP release from astrocytes. We adopted the previously reported "sniffer patch" assay (Hayashi et al., 2004), in which HEK293T cells expressing the ATP-sensitive cation channel P2X7 were used as sniffer cells to generate inward currents in real time in response to ATP released from a closely positioned astrocyte. The sniffer cells showed ATP-evoked currents in a dose-dependent manner (Figures S3A and S3B). We patch-clamped the sniffer cell in whole-cell configuration, while mechanically poking the neighboring astrocytes. Interestingly, poking the cell surface of the Ctrl astrocytes resulted in repeatable inward currents from the sniffer cells recorded at −70 mV (Figures 3A and 3B). Importantly, the currents were drastically reduced when the cKO astrocytes were similarly poked (Figures 3A and 3B). Poking neither the Ctrl nor cKO astrocytes generated currents from EGFP-vector-transfected Ctrl cells (Figure 3B), suggesting specific detection of ATP by the P2X7-expressing sniffer cells.

To further confirm that Piezo1 mediates ATP release from astrocytes, we puffed Yoda1 to activate Piezo1 in astrocytes and recorded currents from the neighboring sniffer cells (Figures 3C and S3C). Sniffer ATP currents were detected in the Ctrl astrocyte group but not in the cKO group (Figures 3C and S3C). Using a newly developed genetically encoded fluorescent GPCR activation-based ATP sensor $GRAB_{ATP1.0}$ that couples the binding of ATP to the human P2Y1 scaffold to

Please cite this article in press as: Chi et al., Astrocytic Piezo1-mediated mechanotransduction determines adult neurogenesis and cognitive functions, Neuron (2022), https://doi.org/10.1016/j.neuron.2022.07.010

CellPress

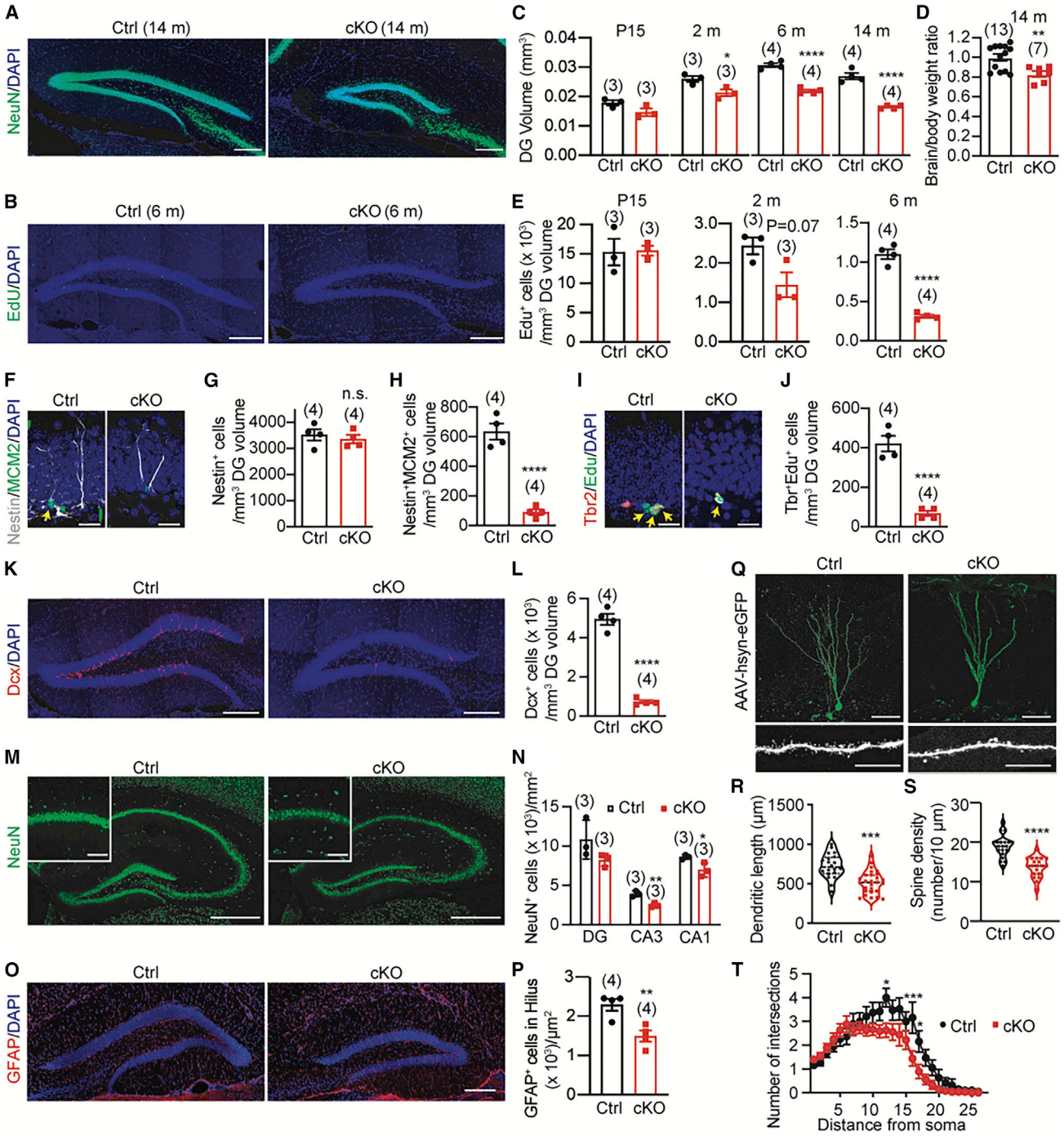

Figure 4. Astrocytic deletion of Piezo1 causes severe reduction of DG volume, brain weight, impaired adult hippocampal neurogenesis, maturation of DG neurons, and reduction of astrocyte number

(A) Representative NeuN- and DAPI-stained images of the DG structure derived from 14-month-old littermate mice. Scale bars, 200 μm.

(B) Representative EdU- and DAPI-stained images of the DG structure derived from 6-month-old littermate mice. Scale bars, 200 μm.

(C) Scatterplot of DG volume derived from littermate mice with the indicated age. Each bar represents mean ± SEM, and the tested mouse number is labeled above the bar. Unpaired Student's t test. *$p < 0.05$, ****$p < 0.0001$.

(D) Scatterplot of brain weight to body weight ratio of 14-month-old littermate mice. Each bar represents mean ± SEM, and the tested mouse number is labeled above the bar. Unpaired Student's t test. **$p < 0.001$.

(E) Scatterplot of EdU-positive proliferating adult hippocampal NSCs in 6-month-old littermate mice. Each bar represents mean ± SEM, and the tested mouse number is labeled above the bar. Unpaired Student's t test. ****$p < 0.0001$.

(legend continued on next page)

fluorescent change of the inserted circularly permuted EGFP (Wu et al., 2022), we verified Yoda1-evoked ATP release from the Ctrl astrocytes, which was drastically reduced in the cKO astrocytes or upon removal of extracellular Ca^{2+} (Figures S3D and S3E). By contrast, the response to externally applied ATP was not affected by the deletion of Piezo or removal of extracellular Ca^{2+} (Figure S3F).

To test whether Piezo1 might respond to other forms of mechanical stimuli to release ATP, we used a bioluminescent ATP assay kit to quantitatively measure ATP released into the extracellular medium in astrocyte cultures, which were subjected to fluid shear stress stimulation via orbital shaking. The extracellular ATP level in the cKO astrocyte cultures was quantitatively lower than that of the Ctrl cells (Figure 3D). Taken together, these independent assays demonstrate that different forms of mechanical stimuli and Yoda1 can cause Piezo1-dependent ATP release from astrocytes.

Previous studies have shown astrocytic ATP release depends on connexin/pannexin channels and TRPV4 channels (Turovsky et al., 2020). Consistently, we found that pharmacologically blocking connexin/pannexin channels and gap junctions with 100 μM carbenoxolone or TRPV4 with 10 μM HC-067047 reduced MA ATP release (Figure 3E). Given that pannexin channels are not intrinsically sensitive to membrane stretch (López et al., 2021), and that TRPV4 channels do not respond to mechanical poking stimuli (Servin-Vences et al., 2017), we hypothesized that these channels might function as necessary components downstream of Piezo1-mediated ATP release. Indeed, it has been shown that the activation of pannexin1 channels depends on Piezo1-mediated calcium signaling (López et al., 2021) and that TRPV4 functions downstream of Piezo1 (Swain et al., 2022). To demonstrate MA ATP release from astrocytes is directly mediated by Piezo1 mechanosensitivity, we employed the mechano-insensitive but Yoda1-responsive Piezo1-ΔEL15-16 mutant in which the extracellular loop connecting the transmembrane (TM) 15 to TM16 is deleted (Zhao et al., 2018). Expression of the full-length Piezo1, but not the Piezo1-ΔEL15-16 mutant, conferred MA currents and ATP release in the cKO astrocytes (Figures 3F and 3H). By contrast, Yoda1-evoked Ca^{2+} response and ATP release in the cKO astrocytes were rescued by the expression of either Piezo1 or the mutant (Figures 3G and 3I). These data demonstrate that the MA currents and ATP release in astrocytes are indeed mediated by the mechanosensitivity of Piezo1.

Astrocytic Piezo1 controls hippocampal structure and *in vivo* neurogenesis

Given that Piezo1 is expressed in the exploratory processes and mediates MA cationic currents, Ca^{2+} influx, and ATP release in astrocytes (Figures 1–3 and S1–S3), we propose that the fully specialized mechanosensory Piezo1 might function as a *bona fide* mechanotransduction channel to enable hippocampal astrocytes to sense their mechanical environments to regulate *in vivo* neurogenesis. Therefore, we examined the hippocampal structure derived from the Ctrl and cKO littermates at post-natal day 15 (P15) and 2, 6, and 14 months old, respectively. Compared with the Ctrl mice, whereas no significant reduction in the DG volume was observed at P15, the cKO mice showed a progressive reduction in their DG volume at 2, 6, and 14 months old (Figures 4A–4C). Remarkably, the 14-month-old cKO mice had an averaged ~40% loss of their DG volume and a striking ~20% reduction in their brain weight to body weight ratio (Figures 4A, 4C, and 4D). The 6-month-old cKO mice also had a significantly reduced cortical area, length, and thickness (Figures S4A–S4D). Immunostaining of molecular markers of the six layers of the cortex revealed reduced $CUX1^+$ or $SATB2^+$

(F) Representative nestin-, MCM2-, and DAPI-stained images of the activated NSCs in DG derived from 6-month-old littermate mice. Yellow arrow indicates nestin- and MCM2-positive active NSCs. Scale bars, 20 μm.
(G) Scatterplot of nestin-positive NSCs in 6-month-old littermate mice. Each bar represents mean ± SEM, and the tested mouse number is labeled above the bar. Unpaired Student's t test. n.s. indicates non-significance.
(H) Scatterplot of nestin- and MCM2-positive active NSCs in 6-month-old littermate mice. Each bar represents mean ± SEM, and the tested mouse number is labeled above the bar. Unpaired Student's t test. ****$p < 0.0001$.
(I) Representative EdU-, Tbr2-, and DAPI-stained images of the progenitor cells in DG derived from 6-month-old littermate mice. Yellow arrow indicates Edu- and Tbr2-positive neural progenitor cells. Scale bars, 20 μm.
(J) Scatterplot of Edu- and Tbr2-positive neural progenitor cells in 6-month-old littermate mice. Each bar represents mean ± SEM, and the tested mouse number is labeled above the bar. Unpaired Student's t test. ****$p < 0.0001$.
(K) Representative Dcx- and DAPI-stained images of the immature neuron in DG derived from 6-month-old littermate mice. Scale bars, 200 μm.
(L) Scatterplot of Dcx-positive immature DG neurons in 6-month-old littermate mice. Each bar represents mean ± SEM, and the tested mouse number is labeled above the bar. Unpaired Student's t test. ****$p < 0.0001$.
(M) Representative NeuN-stained images of the hippocampal structure derived from 6-month-old littermate mice. Scale bars, 100 μm for the upper left and 500 μm for the lower right.
(N) Scatterplot of NeuN-positive mature DG neurons in the DG, CA3, and CA1 areas of 6-month-old littermate mice. Each bar represents mean ± SEM, and the tested mouse number is labeled above the bar. Unpaired Student's t test. *$p < 0.05$, **$p < 0.01$.
(O) Representative GFAP- and DAPI-stained images of the DG structure derived from 6-month-old littermate mice. Scale bars, 200 μm.
(P) Scatterplot of the number of astrocytes in the hilus of DG from 6-month-old littermate mice. Each bar represents mean ± SEM, and the tested mouse number is labeled above the bar. Unpaired Student's t test. **$p < 0.01$.
(Q) EGFP-encoding AAV_9-hsyn-EGFP were steriotaxically injected into the DG area of 6-month-old littermate mice under the indicated treatment conditions. Representative images of sparsely labeled DG granule cells in Ctrl and cKO mice analyzed 4 weeks after injection. The lower panels show dendritic spines. Scale bars, 50 and 10 μm for the top and lower panels, respectively.
(R) Quantification of the total dendritic length of EGFP-positive newborn DG granule cells. Unpaired Student's t test. ***$p < 0.001$.
(S) Quantification of the spine density of EGFP-positive newborn DG neurons. Unpaired Student's t test. ***$p < 0.001$.
(T) Quantification of the number of dendritic branch intersections along the distance from the soma of EGFP-positive newborn DG granule cells. Unpaired Student's t test. *$p < 0.05$, ***$p < 0.001$.

neurons, increased FOXP2$^+$ neurons, and unchanged CTIP2$^+$ neurons in the cKO cortex, indicating that Piezo deletion differentially affect neurons residing in the distinct layers (Figures S4E and S4F).

To examine whether the drastic Piezo1-deletion-induced change in DG volume might be due to defective adult neurogenesis, we assessed the incorporation of EdU in the SGZ of the hippocampus of the Ctrl and cKO mice at P15 and 2 and 6 months old (Figure 4B). Stereological analysis showed that EdU-positive cells in the cKO mice were unchanged at P15, modestly decreased at 2 months old, but significantly reduced at 6 months old (1,103 ± 61 versus 313 ± 19-cells/mm^3 DG volume for Ctrl versus cKO) (Figures 4B and 4E). These data suggest that Piezo deletion in astrocytes causes severely impaired hippocampal neurogenesis from post-adolescent to adult but has a limited effect on post-natal development of the hippocampus.

We next examined the effect of Piezo1 deletion on the sequential steps of adult neurogenesis, including the pool of NSCs marked by nestin staining, active NSCs marked by co-staining of nestin and the mini-chromosome maintenance complex 2 (MCM2) (Figures 4F–4H), neural progenitors marked by co-staining of EdU and Tbr2 (Figures 4I and 4J), immature neurons marked by doublecortin (Dcx) staining (Figures 4K and 4L), and mature neurons by NeuN staining (Figures 4M and 4N). Quantitative analysis showed that the number of nestin-positive NSCs was similar between the Ctrl and cKO mice, indicating an unaltered pool of NSCs upon Piezo1 deletion in astrocytes (Figures 4F and 4G). However, the numbers for active NSCs (Nestin$^+$/MCM2$^+$) (Figures 4F and 4H), neural progenitor cells (Tbr2$^+$/Edu$^+$) (Figures 4I and 4J), and immature neurons (Dcx$^+$) (Figures 4K and 4L) were all drastically reduced in the cKO mice. The number of mature neurons (NeuN$^+$) was also reduced in DG, CA3, and CA1 regions (Figures 4M and 4N). The decreased neuron number was not due to increased apoptosis in the cKO mice (Figure S4G). Furthermore, we found that the cKO mice had a significantly reduced number of astrocytes in the hilus, which might also contribute to the reduced DG volume (Figures 4O and 4P).

Although no Piezo1 expression and MA currents were detected in cultured NSCs (Figures S2C and S2D), we wanted to rule out that any undetectable level of Piezo1 in NSCs might contribute to the impaired *in vivo* neurogenesis in the cKO mice. To this end, we injected retrovirus encoding either EGFP or EGFP-2A-Cre into left and right DG areas of the P1/P2$^{fl/fl}$ Ctrl mice to specifically infect mitotic cells and assayed the impact on adult neurogenesis (Figures S5A–S5G). Analyzing EdU labeling in EGFP-positive cells 3 days post injection revealed no difference in the proliferation of NSCs expressing either EGFP or EGFP-2A-Cre (Figures S5H and S5I), suggesting that deletion of Piezo genes in NSCs did not affect *in vivo* neurogenesis. Together, these data support that Piezo1 expressed in astrocytes plays a prominent role in promoting the proliferation and neurogenesis of NSCs.

We further examined the role of astrocytic Piezo1 on the dendritic outgrowth of DG granule neurons in adult mice by using a GFP-expressing adeno-associated virus (AAV) for sparse labeling (Figure 4Q). Quantitative analysis showed that the GFP-positive granule cells in the cKO mice had significantly reduced dendritic length, spine density, and branching (Figures 4Q–4T). By contrast, the morphology, process length, and number of branches were not affected in the cKO astrocytes (Figures S4H–S4J). Thus, these data suggest that astrocytic Piezo1 also regulates the plasticity of matured DG granule neurons.

Astrocytic Piezo1 promotes ATP-dependent proliferation of NSCs

To test whether astrocytic Piezo1 directly promotes proliferation of NSCs, we examined the effect of either the Ctrl or cKO astrocytes on the proliferation of co-cultured wild-type NSCs. We first verified active proliferation of mouse NSCs cultured alone by assaying EdU incorporation and Sox2 labeling of proliferative NSCs and progenitor cells (Figure S6A). Consistent with previously reported promotional effect of astrocytes on the proliferation of NSCs (Song et al., 2002), co-culture of the Ctrl astrocytes with mouse NSCs resulted in significantly more EdU-positive proliferated NSCs than the Ctrl group without astrocytes (Figures 5A, 5B, and S6B). Remarkably, such effect was totally abolished when NSCs were co-cultured with the cKO astrocytes (Figures 5A and 5B). To test whether the effect of astrocytic Piezo1 on promoting NSC proliferation depends on its channel activities, we applied the spider toxin GxMTx4, a relatively specific blocker of Piezo channels (Bae et al., 2011), to the culture. Interestingly, the application of GsMTx4 blocked the potentiating effect of the Ctrl astrocytes on proliferation of the co-cultured NSCs (Figures 5A and 5B). By contrast, GsMTx4 had no effect on NSCs either cultured alone or co-cultured with the cKO astrocytes (Figures 5A and 5B), indicating its specific role in blocking astrocytic Piezo1 channel activities rather than having any effect on NSCs themselves. In line with this, we found that retrovirus-mediated expression of EGFP-2A-Cre and consequent deletion of Piezo1 and Piezo2 genes in P1/P2$^{fl/fl}$ NSCs affected neither proliferation (Figures S6C and S6D) nor differentiation into neurons and astrocytes (Figures S6E–S6G). Together, these data demonstrate that Piezo1 channel activity in astrocytes is required for promoting proliferation of co-cultured NSCs.

Mechanical activation of Piezo1 in astrocytes can trigger the release of ATP (Figure 3), which is known to promote proliferation of NSCs (Suyama et al., 2012). Indeed, supplementation of the ATP-hydrolyzing enzyme apyrase to degrade extracellular ATP prevented the promoting effect of astrocytes on proliferation of the co-cultured NSCs, but it had no effect on NSCs cultured alone (Figure 5C). We next asked whether the defective effect of the cKO astrocytes on promoting proliferation of co-cultured NSCs could be rescued by ATP supplementation into the culture medium. Interestingly, ATP application resulted in potentiation of NSC proliferation to a similar extent among the three cultured groups, including NSCs alone, co-culture of the Ctrl astrocytes and NSCs, and co-culture of the cKO astrocytes and NSCs (Figures 5A and 5B). The observation that ATP supplementation did not cause additional potentiation of NSC proliferation in the co-cultured group of the Ctrl astrocytes and NSCs suggests that tonic release of ATP from astrocytes is sufficient in mediating the promoting effect of astrocytes on proliferation of NSCs (Figures 5A and 5B).

Please cite this article in press as: Chi et al., Astrocytic Piezo1-mediated mechanotransduction determines adult neurogenesis and cognitive functions, Neuron (2022), https://doi.org/10.1016/j.neuron.2022.07.010

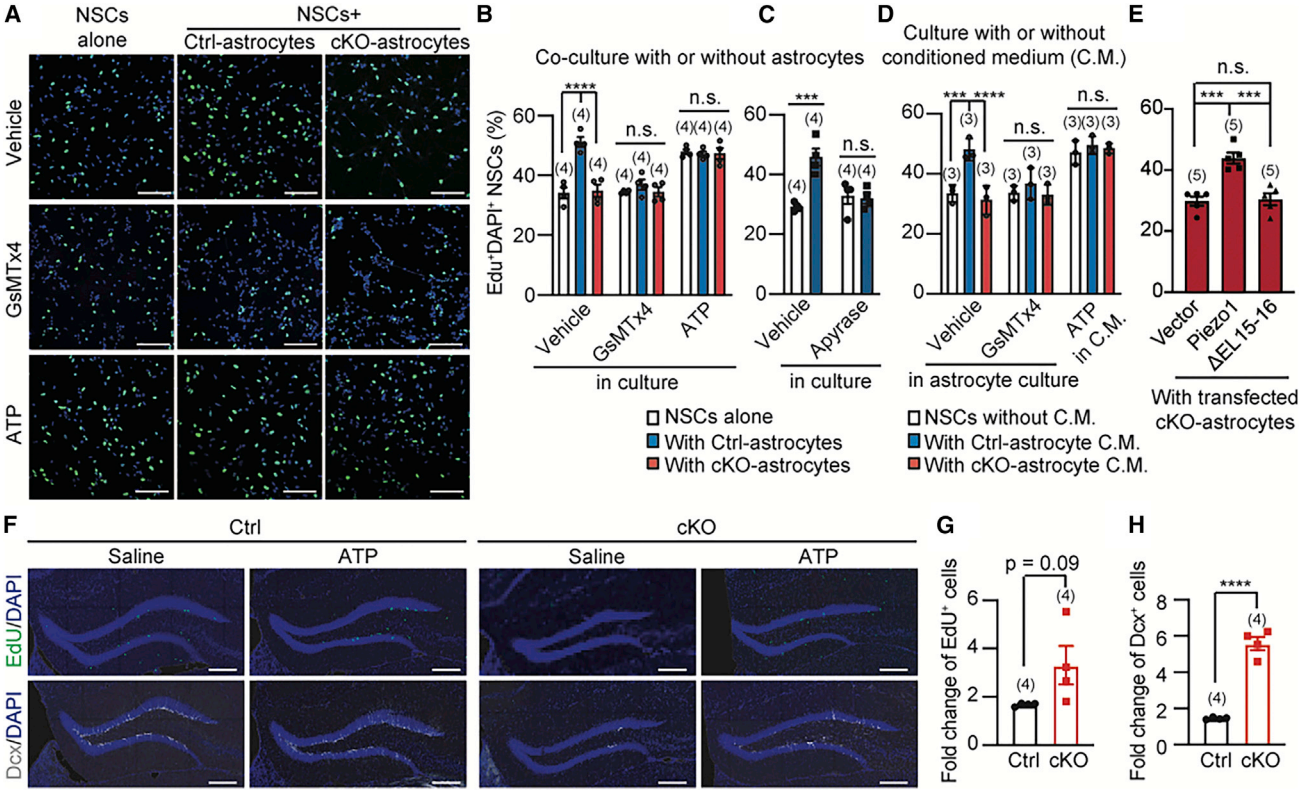

Figure 5. Astrocytic Piezo1 promotes ATP-dependent proliferation of NSCs

(A) Representative EdU-labeled images of proliferating NSCs cultured alone or co-cultured with the indicated astrocytes under the indicated treatment conditions. Scale bars, 100 μm.

(B and C) Scatterplot of EdU-positive proliferating NSCs under the indicated conditions. Each bar represents mean ± SEM, and the number of repeats is labeled above the bar. One-way ANOVA for (B) and unpaired Student's t test for (C). ***p <0.001, ****p <0.0001.

(D) Scatterplot of EdU-positive proliferating NSCs cultured without or with the indicated conditioned medium. ATP was directly added to the conditioned medium. Each bar represents mean ± SEM, and the number of repeats is labeled above the bar. One-way ANOVA. ***p < 0.001, ****p < 0.0001.

(E) Scatterplot of EdU-positive proliferating NSCs cultured with the cKO astrocytes transfected with the indicated constructs. Each bar represents mean ± SEM, and the number of repeats is labeled above the bar. One-way ANOVA. ***p < 0.001.

(F) Representative EdU-labeled and Dcx-immunostained images of hippocampal slices derived from the indicated littermate mice treated with either saline or ATP. Scale bars, 200 μm.

(G and H) Scatterplot of ATP-induced fold change of EdU-positive proliferating NSCs (G) and Dcx-positive immature neurons (H) in the SGZ of the indicated littermate mice. Each bar represents mean ± SEM, and the tested mouse number is labeled above the bar. Unpaired Student's t test. ****p < 0.0001.

To further test whether Piezo1-mediated release of ATP from astrocytes is responsible for promoting NSC proliferation, we subjected NSCs to the conditioned medium from either the Ctrl or cKO astrocytes with or without the application of GsMTx4. Compared with NSCs cultured without conditioned medium, those supplemented with conditioned medium derived from the Ctrl astrocytes, but not from the cKO astrocytes, showed significantly increased proliferation (Figure 5D). Furthermore, GsMTx4 treatment abolished the potentiation effect of conditioned medium derived from the Ctrl astrocytes (Figure 5D). These data are consistent with the idea that Piezo1 channel activity-mediated ATP release from astrocytes promotes NSC proliferation. Similarly to the co-culture experiment, direct addition of ATP to conditioned medium resulted in similar potentiation of NSC proliferation in the three cultured groups, including NSCs without conditioned medium, NSCs with conditioned medium from the Ctrl astrocytes, and NSCs with conditioned medium from the cKO astrocytes (Figure 5D), again suggesting the sufficient role of ATP in promoting NSC proliferation.

To test whether the mechanosensitivity of Piezo1 is required for potentiation of NSC proliferation by the co-cultured astrocytes, we co-cultured NSCs with the cKO astrocytes transfected with either vector, Piezo1, or the Piezo1-ΔEL15-16 mutant. Interestingly, only the expression of Piezo1, but not the mechano-insensitive Piezo1-ΔEL15-16 mutant, potentiated the proliferation of the co-cultured NSCs (Figure 5E). These data suggest that the mechanosensitivity of Piezo1 in astrocytes is required to potentiate the proliferation of NSCs.

We next tested whether ATP is able to rescue the impaired *in vivo* neurogenesis in the cKO mice. We used a mini-osmotic pump to apply either the saline Ctrl or ATP to the DG region of the Ctrl and cKO mice for 2 weeks, then injected EdU for assaying proliferation of adult NSCs. Compared with the saline-treated Ctrl, ATP application caused a substantial increase in

EdU-positive proliferating NSCs and Dcx-positive newborn immature neurons in the cKO mice (Figures 5F–5H). The potentiation effect of ATP on adult neurogenesis in the cKO mice is more robust than that in the Ctrl mice (Figures 5F–5H). For instance, the ATP-induced fold increase of EdU-positive NSCs and Dcx-positive neurons for the Ctrl and cKO mice is 1.7 versus 3.3 and 1.5 versus 5.6, respectively. Furthermore, the ATP-potentiated neurogenesis in the cKO mice was nearly recovered to that of the saline-treated Ctrl mice (Figure 5F). These data, together with the observed sufficient role of ATP in mediating the astrocytic Piezo1-dependent promotion of NSC proliferation in the co-culture experiment (Figures 5A–5D), suggest that the cKO mice might have an ATP-dependent defect of *in vivo* neurogenesis, which is largely rescued upon exogenous ATP supplementation. Previous studies have shown that intraperitoneal injection of ATP could increase the hippocampal ATP level and consequently rescue hippocampal neurogenesis in the dn-SRARE mice, which have defective ATP release from astrocytes (Cao et al., 2013). Therefore, astrocytic Piezo1 might play a critical role in promoting ATP-dependent neurogenesis both *in vitro* and *in vivo*.

Astrocytic Piezo1 impacts learning and memory behaviors and hippocampal long-term potentiation (LTP)

Adult hippocampal neurogenesis confers plasticity to the mature mammalian brain and consequently contributes to learning and memory behaviors. On the basis of the age-dependent progressive reduction of DG volume, and impairment of hippocampal neurogenesis and maturation of newborn DG neurons (Figure 4), we went on to test the behavioral performance of male Ctrl and cKO littermate mice at 6 to 8 months old. The Ctrl and cKO mice had no difference in body weight and behaved similarly in open-field test, suggesting normal locomotion, anxiety, and general exploratory behaviors (Figures S7A–S7D). To examine their learning and memory performance, we carried out the classical Morris water maze (MWM) and Y-maze tests to specifically assay their hippocampal-dependent spatial reference memory and spatial working memory, respectively. Importantly, the cKO mice showed specific deficits in learning and memory behaviors in the MWM test (Figures 6A and 6B). Furthermore, the cKO mice showed a significantly reduced percentage of correct alternative rate, but unaltered total entry time in the Y-maze assay (Figures 6C and 6D), indicating impaired spatial working memory. Collectively, these behavioral analyses suggest that astrocytic Piezo1 plays a critical role in learning and memory formation.

We next examined the impact of astrocyte Piezo1 on hippocampal long-term potentiation (LTP), which is the mechanistic basis of learning and memory and known to be actively regulated by astrocytic activation (Adamsky et al., 2018). Compared with theta burst stimulation (TBS)-induced increase of the extracellular field excitatory postsynaptic potentials (fEPSPs) and LTP response of hippocampal slices derived from the Ctrl mice (Figures 6E and S7E), the cKO slices displayed dampened propensity for maintaining LTP (Figures 6E and 6F). The averaged fEPSP slope during the last 30-min period of the LTP was significantly lower in the cKO (127.7% ± 9.6%) than in the Ctrl slices (182.8% ± 6.9%) (Figures 6E and 6F). To test whether Piezo1-facilitated LTP depends on its channel activities, we applied GsMTx4 during TBS-induced LTP production. GsMTx4 specifically blocked LTP in the Ctrl slices, but it had no effect on the already dampened LTP in the cKO slices (Figures 6G, 6H, and S7F). Together, these data demonstrate that Piezo1 channel activities in astrocytes play a tonic role in regulating neuronal plasticity.

To test whether Piezo1-dependent LTP relies on ATP release from astrocytes, we applied apyrase to degrade extracellular ATP. Apyrase almost completely blocked the LTP in the Ctrl hippocampal slice from an averaged fEPSP slope of 200.1% ± 11.8% to 104.5% ± 7.5% (Figures 6I, 6J, and S7G), a level comparable to that observed in the cKO slices. By contrast, apyrase had no effect on the already impaired LTP in the cKO slices (Figures 6K, 6L, and S7H). Reversely, a direct supplementation of ATP nearly rescued the impaired LTP in the cKO slices to that measured in the Ctrl slices (Figures 6K, 6L, and S7H), while there is no further potentiating effect on the Ctrl slices (Figures 6I, 6J, and S7G), indicating an acute effect of ATP on LTP production in the cKO mice. Together, these data demonstrate that Piezo1-dependent tonic release of ATP from astrocytes plays a critical role in hippocampal LTP production.

Increased Piezo1-mediated mechanotransduction in astrocytes sufficiently enhances LTP and cognitive functions

We generated the transgenic mice overexpressing the GFP-Piezo1 fusion protein (defined as P1-TG) by crossing our previously reported Piezo1-TG$^{\text{fl-mCherry-stop-fl}}$ mice (in which the upstream floxed mCherry coding sequence with a stop codon blocks the translation of the downstream EGFP-Piezo1 fusion protein, defined as Ctrl-TG) (Zhang et al., 2019) with the hGFAP-Cre mouse line. We observed a strong bush-like expression pattern of EGFP-Piezo1 in the GFAP-marked astrocytes residing in the molecular layer of the DG area (Figures 7A and 7B). By contrast, no EGFP-Piezo1 was detected in hippocampal NSCs and granule neurons in the granule cell layer (Figures 7A and 7B). Astrocytes form characteristic endfeet to wrap up blood vessels for responding to and regulating brain vascular tone. Interestingly, EGFP-Piezo1 was clearly co-localized with the endfeet marker protein aquaporin 4 (AQP4), the blood vessel endothelial marker claudin-5, and the pericyte marker PDGFRβ (Figures S8A and S8B), demonstrating its localization at the endfeet of astrocytes. Consistent with the overexpression of Piezo1 in astrocytes, cultured P1-TG astrocytes had markedly enhanced MA currents (Figures 7C and S8C) and Yoda1-induced Ca^{2+} responses (Figures S8D and S8E), suggesting increased mechanotransduction in the P1-TG astrocytes. By contrast, no MA currents were observed in neurons derived from the P1-TG mice (Figure S8F). Taken together, our data demonstrate that Piezo1 is specifically overexpressed in astrocytes at distinct locations, including soma, fine processes, and endfeet, and enhances mechanotransduction.

The DG volume and adult neurogenesis were similar between the Ctrl and P1-TG mice (Figures S8G–S8I). Interestingly, hippocampal slices derived from the P1-TG mice showed increased LTP compared with those derived from the Ctrl-TG mice slices (229.5% ± 17.1% versus 168.9% ± 12.2) (Figures 7D, 7E, and

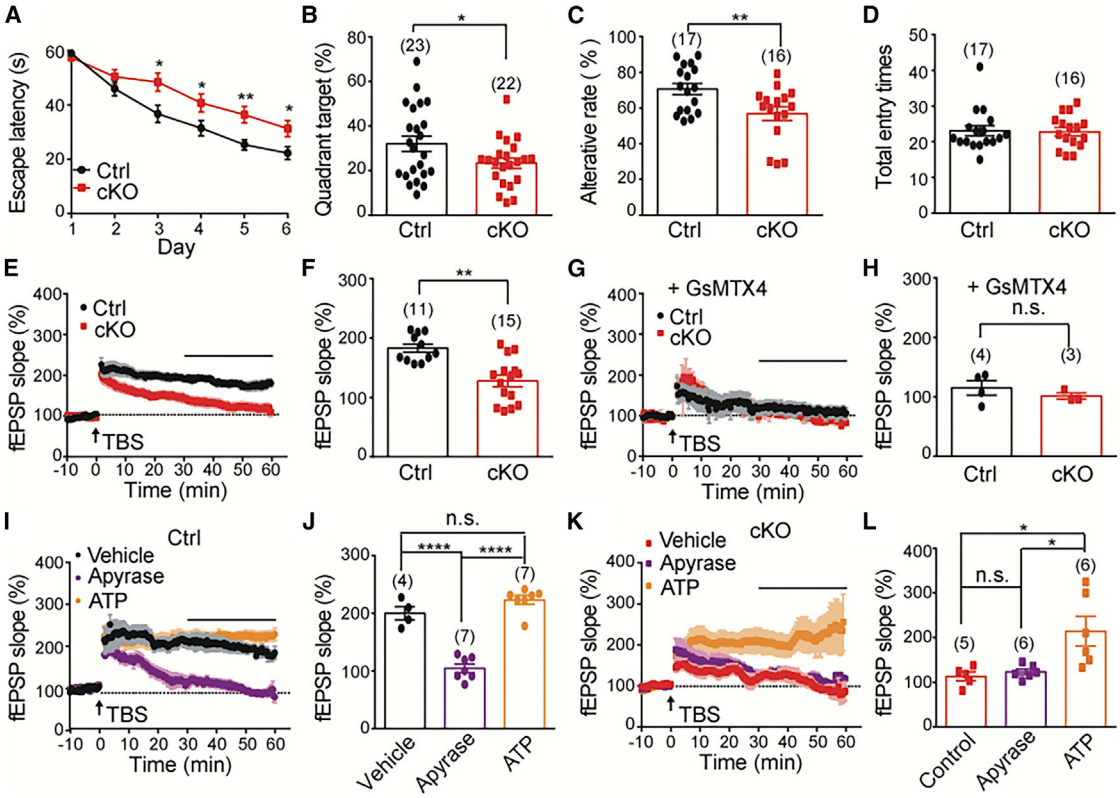

Figure 6. Astrocytic deletion of Piezo1 causes defective learning, memory, and LTP

(A) Escape latency of the indicated littermate male mice to the hidden platform during the training of the standard Morris water maze task. Each data point represents mean ± SEM. Unpaired Student's t test. *p < 0.05, **p < 0.01.

(B) Percentage of time that the indicated male mice spent in the quadrant target area during the probe trial. Each bar represents mean ± SEM, and the tested mouse number is labeled above the bar. Unpaired Student's t test. *p < 0.05.

(C) Percentage of alterative rate of the indicated male mice subjected to the Y-maze test. Each bar represents mean ± SEM, and the tested mouse number is labeled above the bar. Unpaired Student's t test. **p < 0.01.

(D) Total entry time of the indicated male mice subjected to the Y-maze test. Each bar represents mean ± SEM, and the tested mouse number is labeled above the bar. Unpaired Student's t test.

(E, G, I, and K) Average of normalized field EPSP (fEPSP) recorded from the indicated hippocampal slice under the indicated conditions before and after TBS application, indicated by the arrow.

(F, H, J, and L) Scatterplot of the fEPSP slope averaged from the last 30 min of the corresponding recordings shown in (E), (G), (I), and (K), respectively. Each bar represents mean ± SEM, and the recorded slice number is labeled above the bar. Unpaired Student's t test for (F) and (H) and one-way ANOVA for (J) and (L). *p < 0.05, **p < 0.01, ****p < 0.0001.

S8N). Furthermore, while having similar body weight and behaving similarly in open-field test (Figures S8J–S8M), the P1-TG mice outperformed the Ctrl-TG littermates at 5 to 6 months old in both the MWM and Y-maze tests, suggesting enhanced learning and memory performance upon overexpression of Piezo1 in astrocytes (Figures 7F–7I). Taken together, these data demonstrate that overexpression of Piezo1 in astrocytes is sufficient to enhance astrocytic mechanotransduction, hippocampal LTP, and learning and memory behaviors, which appear to be independent of changes in brain structure and adult neurogenesis.

DISCUSSION

By focusing on adult hippocampal neurogenesis that occurs in the unique microenvironment of the SGZ niche and the known regulatory role of astrocytes in LTP and cognitive functions, we here demonstrate that the *bona fide* mechano-gated Piezo1 channel necessarily and sufficiently mediates mechano-chemo transduction in astrocytes (Figures 1, 2, and 3); consequently, it robustly regulates *in vivo* and *in vitro* adult hippocampal neurogenesis (Figures 4 and 5), LTP, and learning and memory behaviors (Figures 6 and 7), highlighting the importance of mechano-gated ion channel-mediated mechanotransduction in adult brain structure and function. Despite that Ca^{2+} signaling has long been postulated to be critical for astrocyte function (Bazargani and Attwell, 2016), to the best of our knowledge, we here not only identify Piezo1 as the endogenous Ca^{2+}-permeable channel mediating spontaneously occurred Ca^{2+} transients in astrocytes but also demonstrate the necessary and sufficient role of endogenous Ca^{2+} signaling in determining astrocyte function *in vivo*, providing compelling evidence to support the concept that

Please cite this article in press as: Chi et al., Astrocytic Piezo1-mediated mechanotransduction determines adult neurogenesis and cognitive functions, Neuron (2022), https://doi.org/10.1016/j.neuron.2022.07.010

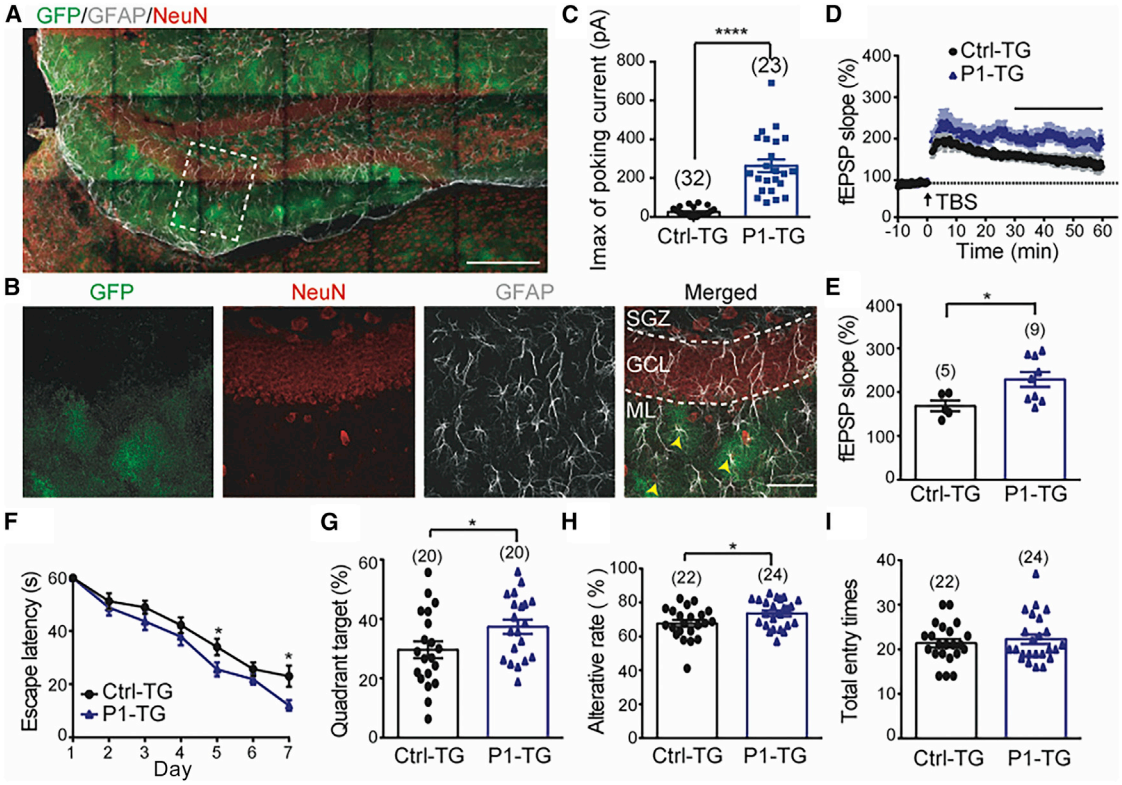

Figure 7. Astrocytic overexpression of Piezo1 promotes LTP, learning, and memory

(A and B) Immunostaining of GFP, GFAP, and NeuN from hippocampal slice derived from the P1-TG mice overexpressing EGFP-Piezo1 fusion proteins. (B) shows the enlarged view of the regions highlighted in the dashed box in (A). Yellow arrow heads indicate astrocytes with bush-like overexpression of EGFP-Piezo1. SGZ, subgranular zone; GCL, granule cell layer; ML, molecular layer. Scale bars: 200 μm for (A) and 50 μm for (B).

(C) Scatterplot of maximal poking currents. Each bar represents mean ± SEM, and the recorded cell number is labeled above the bar. Unpaired Student's t test. ****$p < 0.0001$.

(D) Average of normalized fEPSP recorded from the indicated hippocampal slice for before and after TBS application, indicated by the arrow.

(E) Scatterplot of the fEPSP slope averaged from the last 30 min of the recording shown in (D). Each bar represents mean ± SEM, and the recorded slice number is labeled above the bar. Unpaired Student's t test. *$p < 0.05$.

(F) Escape latency of the indicated male mice to the hidden platform during the training of the standard Morris water maze task. Each data point represents mean ± SEM. Unpaired Student's t test. *$p < 0.05$.

(G) Percentage of time that the indicated male mice spent in the quadrant target area during the probe trial. Each bar represents mean ± SEM, and the tested mouse number is labeled above the bar. Unpaired Student's t test. *$p < 0.05$.

(H) Percentage of alternative rate of the indicated male mice subjected to the Y-maze test. Each bar represents mean ± SEM, and the tested mouse number is labeled above the bar. Unpaired Student's t test. *$p < 0.05$.

(I) Total entry time of the indicated male mice subjected to the Y-maze test. Each bar represents mean ± SEM, and the tested mouse number is labeled above the bar. Unpaired Student's t test.

non-excitable astrocytes actively participate in brain functions via Ca^{2+} signaling mechanisms.

The distinct properties of astrocytes and the fully specialized mechanosensor Piezo1 might enable an ideal mechano-surveillance system to precisely monitor subtle changes of the mechanical environment of the brain (Figure 8). Astrocytes possess the characteristic bush-like morphology with complex fine processes, which forms networks to cover specified non-overlapping surroundings (~13,000 μm^3 for each astrocyte) and exhibits frequent, highly localized and heterogeneous Ca^{2+} transients (Bindocci et al., 2017; Shigetomi et al., 2013a). Our finding that Piezo1 is expressed in the processes and mediates mechanically evoked Ca^{2+} influx in cultured astrocytes and spontaneously occurred astrocytic Ca^{2+} transients in brain slices (Figure 1) supports the hypothesis that astrocytes might utilize Piezo1 to actively explore local mechanical cues to generate localized Ca^{2+} signaling. Piezo1 has an extraordinary mechanosensitivity with a measured T_{50} (the tension required for half maximal activation) of ~1.4–5 mN/m (Cox et al., 2016; Lewis and Grandl, 2015; Syeda et al., 2016) that is within the resting cellular membrane tension (1–2 mN/m) and responds to various forms of mechanical stimulation, including poking, stretching, shear stress, substrate deflection and roughness, and endogenously generated cellular traction force (Xiao, 2020).

The homotrimeric Piezo channel resembles a gigantic three-bladed propeller-like structure (Ge et al., 2015; Guo and MacKinnon, 2017; Saotome et al., 2018; Wang et al., 2019b; Zhao et al., 2018) in which the non-planar TM regions of a total

Please cite this article in press as: Chi et al., Astrocytic Piezo1-mediated mechanotransduction determines adult neurogenesis and cognitive functions, Neuron (2022), https://doi.org/10.1016/j.neuron.2022.07.010

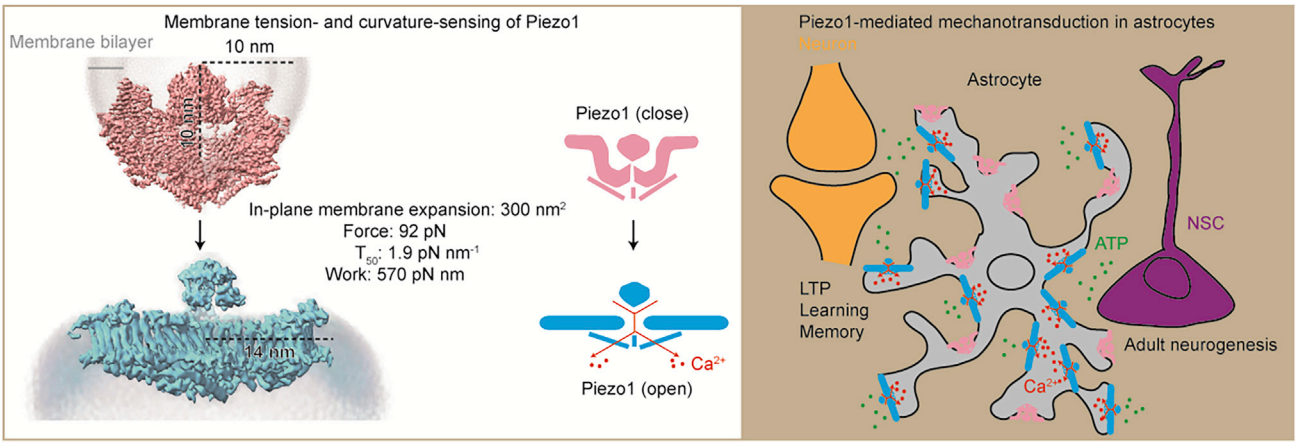

Figure 8. A proposed model for the astrocyte Piezo1-mediated mechano-surveillance system in regulating adult brain functions

The unique structure and mechano-gating mechanism of Piezo1 and the characteristic bush-like morphology of astrocytes might enable an ideal mechano-surveillance system to precisely monitor subtle changes of the mechanical environment of the brain, such as membrane curvature, initiating mechanically evoked Ca^{2+} and ATP signaling to regulate adult hippocampal neurogenesis, neuronal LTP, learning, and memory.

of 114 TM segments (TMs, 38 in each subunit) are collectively curved into a signature nano-bowl shape with an open diameter of 20 nm and a depth of 10 nm (Yang et al., 2022) (Figure 8), which causes the residing membrane to adopt a similarly curved and non-planar shape. Tension-induced flattening of the Piezo-membrane system might provide gating energy to open the channel (Haselwandter and MacKinnon, 2018; Lin et al., 2019). In line with this hypothesis, we have determined the curved and flattened structure of Piezo1 in liposome vesicles, directly visualized the substantial deformability of the Piezo1-lipid bilayer system, and calculated the key parameters upon transition from the curved and closed state to the flattened and open state, including an in-plane membrane areal expansion of 300 nm^2, a force of 92 pN, a half maximal activation tension of 1.9 pN nm^{-1}, and a work of 570 pN (Yang et al., 2022). Thus, such an intrinsic structure-based mechanogating mechanism can confer an exquisite mechanosensitivity to the Piezo channel in response to changes in local membrane curvature and tension. It is possible that the nanoscale fine processes of astrocytes might adopt variable curvatures in response to their mechanical surroundings and consequently gate Piezo1 to control local Ca^{2+} signaling and tonic ATP release (Figure 8). Indeed, it has been shown that astrocytes can sense nanoscale substrate roughness through Piezo1, which in turn alters their own surface roughness suitable for neuronal interaction (Blumenthal et al., 2014). The localization of Piezo1 in the endfeet of astrocytes (Figures S8A and S8B) might also allow the astrocyte-Piezo1 system to directly respond to mechanical changes associated with dilation and constriction of brain blood vessels, which are not only critical components of the neurogenic niche of SGZ but also functionally coupled to neuronal activities. Piezo1 might also sense altered mechanical stiffness of brain tissues, such as β-amyloid (Aβ) plagues in Alzheimer disease, and consequently participate in brain diseases. Future studies might dissect out the specific contributions of astrocytic Piezo1-mediated mechanotransduction, originating from distinct mechanical cues, within the brain to cognitive functions and diseases.

STAR★METHODS

Detailed methods are provided in the online version of this paper and include the following:

- KEY RESOURCES TABLE
- RESOURCE AVAILABILITY
  - Lead contact
  - Materials availability
  - Data and code availability
- EXPERIMENTAL MODEL AND SUBJECT DETAILS
  - Animals
  - Cell lines
  - Primary mouse cell cultures
- METHOD DETAILS
  - RNA extraction and RT-PCR
  - Primary culture of mouse astrocytes and neurons
  - Co-culture of primary mouse NSCs and astrocytes
  - EdU labeling
  - Transient transfection
  - Immunohistochemistry
  - Single-cell Fura-2 Ca^{2+} imaging
  - Two-photon Ca^{2+} imaging of hippocampal slices and data analysis
  - Western blotting
  - Immunofluorescent staining of primarily cultured astrocytes
  - ATP infusion
  - Stereotaxic injections
  - Behavioral studies
  - Field EPSP recordings of hippocampal slices
  - Whole-cell electrophysiology and mechanical indentation stimulation
  - Measurement of ATP release from astrocytes
  - Cell-attached electrophysiology and stretch stimulation
- QUANTIFICATION AND STATISTICAL ANALYSIS

- Cell quantification
- Dendritic morphology analysis
- Dendritic spine quantification
- Data analysis

SUPPLEMENTAL INFORMATION

Supplemental information can be found online at https://doi.org/10.1016/j.neuron.2022.07.010.

ACKNOWLEDGMENTS

We thank Dr. Ardem Patapoutian for sharing the Piezo1$^{fl/fl}$ and Piezo2$^{fl/fl}$ mice; Drs. Yulong Li and Zhaofa Wu for help with the GRAB$_{ATP1.0}$ sensor; Dr. Bai Lu for sharing two-photon microscope; Dr. Zai Chang and other staff at the animal facility center of Tsinghua University for maintaining mice; Jing Wang for initial management of the mice; and Li Wang for constructing the P2X7 plasmid. This work was supported by grants 31825014, 32130049, 2021ZD0203301, and 32021002 to B.X. from either the National Natural Science Foundation of China or the Ministry of Science and Technology of China.

AUTHOR CONTRIBUTIONS

S.C., Y.C., and H.W. contributed equally to this work. S.C. carried out electrophysiology and Ca^{2+} imaging, RT-PCR and immunostaining of primarily cultured cells, measurement of ATP release, hippocampal slice preparation and LTP recordings and data analysis, and mouse management. Y.C. designed experiments and characterized *in vivo* adult neurogenesis and *in vitro* co-culture of astrocytes and NSCs and data analysis. H.W. did behavioral tests, 2-photon Ca^{2+} imaging of brain slices with help from S.C., western blot, and data analysis. J.J. helped with behavioral tests, T.Z. helped with western blot, S.S. helped with the culture of astrocytes, and Z.Z. and Y.Z. provided technical assistance and discussion. B.X. conceived and directed the study, analyzed data, made figures, and wrote the manuscript with the help from all other authors.

DECLARATION OF INTERESTS

The authors declare no competing interests.

Received: June 21, 2021
Revised: May 31, 2022
Accepted: July 12, 2022
Published: August 12, 2022

REFERENCES

Adamsky, A., Kol, A., Kreisel, T., Doron, A., Ozeri-Engelhard, N., Melcer, T., Refaeli, R., Horn, H., Regev, L., Groysman, M., et al. (2018). Astrocytic activation generates de novo neuronal potentiation and memory enhancement. Cell *174*. 59–71.e14.

Araque, A., Carmignoto, G., Haydon, P.G., Oliet, S.H., Robitaille, R., and Volterra, A. (2014). Gliotransmitters travel in time and space. Neuron *81*, 728–739.

Bae, C., Sachs, F., and Gottlieb, P.A. (2011). The mechanosensitive ion channel Piezo1 is inhibited by the peptide GsMTx4. Biochemistry *50*, 6295–6300.

Bazargani, N., and Attwell, D. (2016). Astrocyte calcium signaling: the third wave. Nat. Neurosci. *19*, 182–189.

Bindocci, E., Savtchouk, I., Liaudet, N., Becker, D., Carriero, G., and Volterra, A. (2017). Three-dimensional Ca^{2+} imaging advances understanding of astrocyte biology. Science *356*.

Blumenthal, N.R., Hermanson, O., Heimrich, B., and Shastri, V.P. (2014). Stochastic nanoroughness modulates neuron-astrocyte interactions and function via mechanosensing cation channels. Proc. Natl. Acad. Sci. USA *111*, 16124–16129.

Bond, A.M., Ming, G.L., and Song, H. (2015). Adult mammalian neural stem cells and neurogenesis: five decades later. Cell Stem Cell *17*, 385–395.

Bowman, C.L., Ding, J.P., Sachs, F., and Sokabe, M. (1992). Mechanotransducing ion channels in astrocytes. Brain Res. *584*, 272–286.

Cahalan, S.M., Lukacs, V., Ranade, S.S., Chien, S., Bandell, M., and Patapoutian, A. (2015). Piezo1 links mechanical forces to red blood cell volume. eLife *4*, e07370.

Cao, X., Li, L.P., Qin, X.H., Li, S.J., Zhang, M., Wang, Q., Hu, H.H., Fang, Y.Y., Gao, Y.B., Li, X.W., et al. (2013). Astrocytic adenosine 5′-triphosphate release regulates the proliferation of neural stem cells in the adult hippocampus. Stem Cells *31*, 1633–1643.

Charles, A.C., Merrill, J.E., Dirksen, E.R., and Sanderson, M.J. (1991). Intercellular signaling in glial cells: calcium waves and oscillations in response to mechanical stimulation and glutamate. Neuron *6*, 983–992.

Chi, S., Cai, W., Liu, P., Zhang, Z., Chen, X., Gao, L., Qi, J., Bi, L., Chen, L., and Qi, Z. (2010). Baifuzi reduces transient ischemic brain damage through an interaction with the STREX domain of BKCa channels. Cell Death Dis. *1*, e13.

Chi, S., Xiao, R., Li, Q., Zhou, L., He, R., and Qi, Z. (2009). Suppression of neuronal excitability by the secretion of the lamprey (Lampetra japonica) provides a mechanism for its evolutionary stability. Pflugers Arch. *458*, 537–545.

Coste, B., Mathur, J., Schmidt, M., Earley, T.J., Ranade, S., Petrus, M.J., Dubin, A.E., and Patapoutian, A. (2010). Piezo1 and Piezo2 are essential components of distinct mechanically activated cation channels. Science *330*, 55–60.

Coste, B., Xiao, B., Santos, J.S., Syeda, R., Grandl, J., Spencer, K.S., Kim, S.E., Schmidt, M., Mathur, J., Dubin, A.E., et al. (2012). Piezo proteins are pore-forming subunits of mechanically activated channels. Nature *483*, 176–181.

Cox, C.D., Bae, C., Ziegler, L., Hartley, S., Nikolova-Krstevski, V., Rohde, P.R., Ng, C.A., Sachs, F., Gottlieb, P.A., and Martinac, B. (2016). Removal of the mechanoprotective influence of the cytoskeleton reveals PIEZO1 is gated by bilayer tension. Nat. Commun. *7*, 10366.

Douguet, D., and Honoré, E. (2019). Mammalian mechanoelectrical transduction: structure and function of force-gated ion channels. Cell *179*, 340–354.

Ellefsen, K.L., Holt, J.R., Chang, A.C., Nourse, J.L., Arulmoli, J., Mekhdjian, A.H., Abuwarda, H., Tombola, F., Flanagan, L.A., Dunn, A.R., et al. (2019). Myosin-II mediated traction forces evoke localized Piezo1-dependent Ca^{2+} flickers. Commun. Biol. *2*, 298.

Fiacco, T.A., Agulhon, C., Taves, S.R., Petravicz, J., Casper, K.B., Dong, X., Chen, J., and McCarthy, K.D. (2007). Selective stimulation of astrocyte calcium in situ does not affect neuronal excitatory synaptic activity. Neuron *54*, 611–626.

Ge, J., Li, W., Zhao, Q., Li, N., Chen, M., Zhi, P., Li, R., Gao, N., Xiao, B., and Yang, M. (2015). Architecture of the mammalian mechanosensitive Piezo1 channel. Nature *527*, 64–69.

Geng, J., Liu, W., Zhou, H., Zhang, T., Wang, L., Zhang, M., Li, Y., Shen, B., Li, X., and Xiao, B. (2020). A plug-and-latch mechanism for gating the mechanosensitive piezo channel. Neuron *106*. 438–451.e6.

Gonçalves, J.T., Schafer, S.T., and Gage, F.H. (2016). Adult neurogenesis in the hippocampus: from stem cells to behavior. Cell *167*, 897–914.

Guo, W., Patzlaff, N.E., Jobe, E.M., and Zhao, X. (2012). Isolation of multipotent neural stem or progenitor cells from both the dentate gyrus and subventricular zone of a single adult mouse. Nat. Protoc. *7*, 2005–2012.

Guo, Y.R., and MacKinnon, R. (2017). Structure-based membrane dome mechanism for Piezo mechanosensitivity. eLife *6*, e33660.

Guthrie, P.B., Knappenberger, J., Segal, M., Bennett, M.V., Charles, A.C., and Kater, S.B. (1999). ATP released from astrocytes mediates glial calcium waves. J. Neurosci. *19*, 520–528.

Haselwandter, C.A., and MacKinnon, R. (2018). Piezo's membrane footprint and its contribution to mechanosensitivity. eLife *7*, e41968.

Hayashi, S., Hazama, A., Dutta, A.K., Sabirov, R.Z., and Okada, Y. (2004). Detecting ATP release by a biosensor method. Sci. STKE *2004*, pl14.

Holt, J.R., Zeng, W.Z., Evans, E.L., Woo, S.H., Ma, S., Abuwarda, H., Loud, M., Patapoutian, A., and Pathak, M.M. (2021). Spatiotemporal dynamics of PIEZO1 localization controls keratinocyte migration during wound healing. eLife *10*, e65415.

Jiang, Y., Yang, X., Jiang, J., and Xiao, B. (2021). Structural designs and mechanogating mechanisms of the mechanosensitive piezo channels. Trends Biochem. Sci. *46*, 472–488.

Koizumi, S., Fujishita, K., Tsuda, M., Shigemoto-Mogami, Y., and Inoue, K. (2003). Dynamic inhibition of excitatory synaptic transmission by astrocyte-derived ATP in hippocampal cultures. Proc. Natl. Acad. Sci. USA *100*, 11023–11028.

Lewis, A.H., and Grandl, J. (2015). Mechanical sensitivity of Piezo1 ion channels can be tuned by cellular membrane tension. eLife *4*.

Lin, Y.C., Guo, Y.R., Miyagi, A., Levring, J., MacKinnon, R., and Scheuring, S. (2019). Force-induced conformational changes in PIEZO1. Nature *573*, 230–234.

López, X., Palacios-Prado, N., Güiza, J., Escamilla, R., Fernández, P., Vega, J.L., Rojas, M., Marquez-Miranda, V., Chamorro, E., Cárdenas, A.M., et al. (2021). A physiologic rise in cytoplasmic calcium ion signal increases pannexin1 channel activity via a C-terminus phosphorylation by CaMKII. Proc. Natl. Acad. Sci. USA *118*. e2108967118.

Ma, S., Dubin, A.E., Zhang, Y., Mousavi, S.A.R., Wang, Y., Coombs, A.M., Loud, M., Andolfo, I., and Patapoutian, A. (2021). A role of PIEZO1 in iron metabolism in mice and humans. Cell *184*. 969–982.e13.

Newman, E.A. (2001). Propagation of intercellular calcium waves in retinal astrocytes and Muller cells. J. Neurosci. *21*, 2215–2223.

Pryazhnikov, E., and Khiroug, L. (2008). Sub-micromolar increase in [Ca(2+)](i) triggers delayed exocytosis of ATP in cultured astrocytes. Glia *56*, 38–49.

Ranade, S.S., Qiu, Z., Woo, S.H., Hur, S.S., Murthy, S.E., Cahalan, S.M., Xu, J., Mathur, J., Bandell, M., Coste, B., et al. (2014a). Piezo1, a mechanically activated ion channel, is required for vascular development in mice. Proc. Natl. Acad. Sci. USA *111*, 10347–10352.

Ranade, S.S., Woo, S.H., Dubin, A.E., Moshourab, R.A., Wetzel, C., Petrus, M., Mathur, J., Bégay, V., Coste, B., Mainquist, J., et al. (2014b). Piezo2 is the major transducer of mechanical forces for touch sensation in mice. Nature *516*, 121–125.

Rungta, R.L., Bernier, L.P., Dissing-Olesen, L., Groten, C.J., LeDue, J.M., Ko, R., Drissler, S., and MacVicar, B.A. (2016). Ca^{2+} transients in astrocyte fine processes occur via Ca^{2+} influx in the adult mouse hippocampus. Glia *64*, 2093–2103.

Saotome, K., Murthy, S.E., Kefauver, J.M., Whitwam, T., Patapoutian, A., and Ward, A.B. (2018). Structure of the mechanically activated ion channel Piezo1. Nature *554*, 481–486.

Schildge, S., Bohrer, C., Beck, K., and Schachtrup, C. (2013). Isolation and culture of mouse cortical astrocytes. J. Vis. Exp. 50079.

Servin-Vences, M.R., Moroni, M., Lewin, G.R., and Poole, K. (2017). Direct measurement of TRPV4 and PIEZO1 activity reveals multiple mechanotransduction pathways in chondrocytes. eLife *6*, e21074.

Shigetomi, E., Bushong, E.A., Haustein, M.D., Tong, X., Jackson-Weaver, O., Kracun, S., Xu, J., Sofroniew, M.V., Ellisman, M.H., and Khakh, B.S. (2013a). Imaging calcium microdomains within entire astrocyte territories and endfeet with GCaMPs expressed using adeno-associated viruses. J. Gen. Physiol. *141*, 633–647.

Shigetomi, E., Jackson-Weaver, O., Huckstepp, R.T., O'Dell, T.J., and Khakh, B.S. (2013b). TRPA1 channels are regulators of astrocyte basal calcium levels and long-term potentiation via constitutive D-serine release. J. Neurosci. *33*, 10143–10153.

Shigetomi, E., Kracun, S., Sofroniew, M.V., and Khakh, B.S. (2010). A genetically targeted optical sensor to monitor calcium signals in astrocyte processes. Nat. Neurosci. *13*, 759–766.

Song, H., Stevens, C.F., and Gage, F.H. (2002). Astroglia induce neurogenesis from adult neural stem cells. Nature *417*, 39–44.

Srinivasan, R., Huang, B.S., Venugopal, S., Johnston, A.D., Chai, H., Zeng, H., Golshani, P., and Khakh, B.S. (2015). Ca^{2+} signaling in astrocytes from Ip3r2(−/−) mice in brain slices and during startle responses in vivo. Nat. Neurosci. *18*, 708–717.

Suyama, S., Sunabori, T., Kanki, H., Sawamoto, K., Gachet, C., Koizumi, S., and Okano, H. (2012). Purinergic signaling promotes proliferation of adult mouse subventricular zone cells. J. Neurosci. *32*, 9238–9247.

Swain, S.M., Romac, J.M., Vigna, S.R., and Liddle, R.A. (2022). Piezo1-mediated stellate cell activation causes pressure-induced pancreatic fibrosis in mice. JCI Insight *7*, e158288.

Syeda, R., Florendo, M.N., Cox, C.D., Kefauver, J.M., Santos, J.S., Martinac, B., and Patapoutian, A. (2016). Piezo1 channels are inherently mechanosensitive. Cell Rep. *17*, 1739–1746.

Syeda, R., Xu, J., Dubin, A.E., Coste, B., Mathur, J., Huynh, T., Matzen, J., Lao, J., Tully, D.C., Engels, I.H., et al. (2015). Chemical activation of the mechanotransduction channel Piezo1. eLife *4*, e0736.

Toth, A.B., Hori, K., Novakovic, M.M., Bernstein, N.G., Lambot, L., and Prakriya, M. (2019). CRAC channels regulate astrocyte Ca^{2+} signaling and gliotransmitter release to modulate hippocampal GABAergic transmission. Sci. Signal. *12*, eaaw5450.

Turovsky, E.A., Braga, A., Yu, Y., Esteras, N., Korsak, A., Theparambil, S.M., Hadjihambi, A., Hosford, P.S., Teschemacher, A.G., Marina, N., et al. (2020). Mechanosensory signaling in astrocytes. J. Neurosci. *40*, 9364–9371.

Velasco-Estevez, M., Rolle, S.O., Mampay, M., Dev, K.K., and Sheridan, G.K. (2020). Piezo1 regulates calcium oscillations and cytokine release from astrocytes. Glia *68*, 145–160.

Vicidomini, C., Guo, N., and Sahay, A. (2020). Communication, cross talk, and signal integration in the adult hippocampal neurogenic niche. Neuron *105*, 220–235.

Wang, J., Cui, Y., Yu, Z., Wang, W., Cheng, X., Ji, W., Guo, S., Zhou, Q., Wu, N., Chen, Y., et al. (2019a). Brain endothelial cells maintain lactate homeostasis and control adult hippocampal neurogenesis. Cell Stem Cell *25*. 754–767.e9.

Wang, L., Zhou, H., Zhang, M., Liu, W., Deng, T., Zhao, Q., Li, Y., Lei, J., Li, X., and Xiao, B. (2019b). Structure and mechanogating of the mammalian tactile channel PIEZO2. Nature *573*, 225–229.

Wu, Z., He, K., Chen, Y., Li, H., Pan, S., Li, B., Liu, T., Xi, F., Deng, F., Wang, H., et al. (2022). A sensitive GRAB sensor for detecting extracellular ATP in vitro and in vivo. Neuron *110*. 770–782.e5.

Xiao, B. (2020). Levering mechanically activated Piezo channels for potential pharmacological intervention. Annu. Rev. Pharmacol. Toxicol. *60*, 195–218.

Xiong, Y., Teng, S., Zheng, L., Sun, S., Li, J., Guo, N., Li, M., Wang, L., Zhu, F., Wang, C., et al. (2018). Stretch-induced Ca^{2+} independent ATP release in hippocampal astrocytes. J. Physiol. *596*, 1931–1947.

Yang, X., Lin, C., Chen, X., Li, S., Li, X., and Xiao, B. (2022). Structure deformation and curvature sensing of PIEZO1 in lipid membranes. Nature *604*, 377–383.

Zeisel, A., Hochgerner, H., Lönnerberg, P., Johnsson, A., Memic, F., van der Zwan, J., Häring, M., Braun, E., Borm, L.E., La Manno, G., et al. (2018). Molecular architecture of the mouse nervous system. Cell *174*. 999–1014.e22.

Zhang, M., Wang, Y., Geng, J., Zhou, S., and Xiao, B. (2019). Mechanically activated piezo channels mediate touch and suppress acute mechanical pain response in mice. Cell Rep. *26*. 1419.e4–1431.e4.

Zhang, T., Chi, S., Jiang, F., Zhao, Q., and Xiao, B. (2017). A protein interaction mechanism for suppressing the mechanosensitive Piezo channels. Nat. Commun. *8*, 1797.

Zhao, Q., Wu, K., Geng, J., Chi, S., Wang, Y., Zhi, P., Zhang, M., and Xiao, B. (2016). Ion permeation and mechanotransduction mechanisms of mechanosensitive Piezo channels. Neuron *89*, 1248–1263.

Zhao, Q., Zhou, H., Chi, S., Wang, Y., Wang, J., Geng, J., Wu, K., Liu, W., Zhang, T., Dong, M.Q., et al. (2018). Structure and mechanogating mechanism of the Piezo1 channel. Nature *554*, 487–492.

Zhuo, L., Theis, M., Alvarez-Maya, I., Brenner, M., Willecke, K., and Messing, A. (2001). hGFAP-cre transgenic mice for manipulation of glial and neuronal function in vivo. Genesis *31*, 85–94.

Please cite this article in press as: Chi et al., Astrocytic Piezo1-mediated mechanotransduction determines adult neurogenesis and cognitive functions, Neuron (2022), https://doi.org/10.1016/j.neuron.2022.07.010

STAR★METHODS

KEY RESOURCES TABLE

REAGENT or RESOURCE	SOURCE	IDENTIFIER
Antibodies		
Chicken anti-Nestin (1:500)	Aves Labs	NES; RRID: AB_2314882
Mouse anti-NeuN (1:500)	Millipore	Cat# MAB377; RRID: AB_2298767
Rabbit anti-NeuN (1:1,000)	Cell Signaling Technology	Cat# 12943; RRID:AB_2630395
Goat anti-DCX (1:100)	Santa Cruz Biotechnology	Cat# SC-8066; RRID: AB_2088494
Rabbit anti-DCX (1:500)	Cell Signaling Technology	Cat#4604; RRID: AB_561007
Rabbit anti-GFAP (1:2,000)	Dako	Cat# Z0334; RRID:AB_10013382
Rabbit anti-S100β (1:500)	Abcam	Cat# ab52642 RRID:AB_882426
Chicken anti-GFP (1:1,000)	Invitrogen	Cat# A10262; RRID:AB_2534023
Mouse anti-BM28 (1:500)	BD Bioscience	Cat# 610700; RRID:AB_2141952
Rabbit anti-Tbr2 (1:500)	Abcam	Cat#ab23345; RRID: AB_778267
Rabbit anti-beta3 tubulin (1:500)	Cell Signaling Technology	Cat# 5568S
Rabbit anti-PDGFRβ (1:200)	Cell Signaling Technology	Cat# 3169; RRID:AB_2162497
Rabbit anti-AQP4 (1:500)	Abcam	RRID:AB_955676
Rabbit anti-RFP (1:1000)	Rockland	RRID:AB_2209751
Rabbit anti-Cux1 (1:500)	Proteintech	Cat# 11733-1-AP RRID:AB_2086995
Rabbit anti-Ctip2 (1:500)	Abcam	Cat# ab40636
Rabbit anti-Satb2 (1:500)	Abcam	Cat# ab92446 RRID:AB_10563678
Rabbit anti-Foxp2 (1:500)	Abcam	Cat# ab 172320
Donkey anti-goat 568 (1:500)	Invitrogen	Cat#A11057; RRID: AB_142581
Donkey anti-mouse 568 (1:500)	Invitrogen	Cat#A10037; RRID: AB_2534013
Donkey anti-rabbit 568 (1:500)	Invitrogen	Cat#A10042; RRID: AB_2534017
Donkey anti-Rat 594 (1:500)	Invitrogen	Cat#A21209; RRID: AB_2535795
Donkey anti-rabbit 647 (1:500)	Invitrogen	Cat#A31573; RRID: AB_2536183
Donkey anti goat 647 (1:500)	Invitrogen	Cat# A-21447; RRID: AB_141844
Donkey anti mouse 647 (1:500)	Invitrogen	Cat#A31571; RRID: AB_162542
Donkey anti-Rabbit 488 (1:500)	Invitrogen	Cat#A21206; RRID: AB_141708
Donkey anti-Rat 488 (1:500)	Invitrogen	Cat#A21208; RRID: AB_141709
Donkey anti-Goat 488 (1:500)	Invitrogen	Cat#A11055; RRID: AB_2534102
Donkey anti-Mouse 488 (1:500)	Invitrogen	Cat#A21202; RRID: AB_141607
Donley anti-chicken 488 (1:500)	Invitrogen	Cat# SA1-72000; RRID:AB_923386
Bacterial and virus strains		
Escherichia coli: XL10-Gold Chemical Competent Cell	Homemade	N/A
AAV9-hsyn-EGFP	Taitool	N/A
Lenti-GfaABC1d-EGFP	Taitool	N/A
Retro-CMV-EGFP	Taitool	N/A
Retro-CMV-EGFP-2A-Cre	Taitool	N/A
AAV2/9-GfaABC1D-ATP1.0	Vigene Biosciences (this paper)	N/A
Chemicals, peptides, and recombinant proteins		
Fura-2	Life Technologies	Cat#F1201
Pluronic F-127	Life Technologies	Cat# P3000MP
Dulbecco's Modified Eagle Medium (DMEM)	ThermoFisher	Cat#C11995500BT

(*Continued on next page*)

Continued

REAGENT or RESOURCE	SOURCE	IDENTIFIER
EGM-2 bullet kit	Lonza	Cat#CC-3162
Fetal Bovine Serum (FBS)	ThermoFisher	Cat#10099141C
Neurobasal Medium	GIBCO	Cat#21103-049
Dulbecco's Modified Eagle Medium (DMEM)	GIBCO	Cat#C11995500BT
Dulbecco's Phosphate-Buffered Saline (DPBS)	Biological Industries	02-023-1A
L-Glutamine	GIBCO	Cat#25030-081
0.5% Trypsin-EDTA	GIBCO	Cat#15400-054
HBSS, no Calcium, no Magnesium, no Phenol Red	GIBCO	Cat#14175-095
Antibiotic-Antimycotic	GIBCO	Cat#15240-062
B27 Supplement	GIBCO	Cat#17504-044
Human EGF	PeproTech	Cat#AF-100-15-1000
Human FGF-basic	PeproTech	Cat#AF-100-18B-1000
Yoda1	Pharmacodia	N/A
Fluo-4-AM	Thermo	Cat# F14201
GsMTX4	Tocris Bioscience	N/A
HC-067047	Abcam	Cat#ab145868
Sulforhodamine 101 (SR101)	MedChemExpress	Cat#HY-101878
Critical commercial assays		
AxyPrep Multisource Total RNA Miniprep Kit 250-prep	Axygen	Cat#AP-MN-MS-RNA-250G
iScript cDNS Synthesis Kit	BIO-RAD	Cat#1708890
Micro-osmotic pumps	Alzet	Cat#1007D
Brain Infusion Kit 3	Alzet	Cat#0008851
TSA plus Fluorescence Kit	PerkinElmer	Cat#NEL741001KT
MACS neural tissue dissociation kit	MACS Miltenyi Biotec	Cat#130-092-628
ATP assay kit	Invitrogen	Cat#A22066
Lipofectamine3000 transfection kit	Invitrogen	Cat#L3000015
Experimental models: Cell lines		
HEK293T	Laboratory of Ardem Patapoutian	N/A
Adult mouse hippocampal neural stem cell	This paper	N/A
P0 hippocampal neurons	This paper	N/A
P0 astrocyte	This paper	N/A
Experimental models: Organisms/strains		
Piezo1$^{fl/fl}$ mice	Laboratory of Ardem Patapoutian	N/A
Piezo2$^{fl/fl}$ mice	Laboratory of Ardem Patapoutian	N/A
Piezo1-tdTomato knock-in mouse line	The Jackson Laboratory	Cat# JAX:029214
Piezo1-TG$^{fl\text{-}mCherry\text{-}stop\text{-}fl}$ mice	Zhang et al., 2019	N/A
hGFAP-Cre mice	The Jackson Laboratory	Cat# JAX:004600
Oligonucleotides		
mPiezo1-Forward: TCCTGCTGTATGGGCTGAC	This paper	N/A
mPiezo1-Reverse: AGGGTAGCGTGTGTGTTCC	This paper	N/A
mGAPDH-Forward: ACAATTTCCATCCCAGACC	This paper	N/A
mGAPDH-Reverse:GTGGGTGCAGCGAACTTTAT	This paper	N/A
Recombinant DNA		
Plasmid: full-length mouse Piezo1	Zhao et al., 2018	N/A
Plasmid: Piezo1-ΔEL15-16 mutant	Zhao et al., 2018	N/A
Plasmid: P2X7	This paper	N/A

(*Continued on next page*)

Continued

REAGENT or RESOURCE	SOURCE	IDENTIFIER
Software and algorithms		
pClamp 10.6	Molecular Devices	https://www.moleculardevices.com/products/axon-patch-clamp-system/acquisition-and-analysis-software/pclamp-software-suite
Origin 9.2	OriginLab	http://www.originlab.com/
GraphPad Prism	GraphPad Software Inc	http://www.graphpad.com/scientific-software/prism/

RESOURCE AVAILABILITY

Lead contact

Further information and requests for resources and reagents should be directed to and will be fulfilled by the lead contact, Bailong Xiao (xbailong@mail.tsinghua.edu.cn).

Materials availability

All unique reagents generated in this study are available from the lead contact with a completed Materials Transfer Agreement.

Data and code availability

- All data reported in this paper will be shared by the lead contact upon request.
- This paper does not report original code.
- Any additional information required to reanalyze the data reported in this paper is available from the lead contact upon request.

EXPERIMENTAL MODEL AND SUBJECT DETAILS

Animals

All animal care and procedures were approved and performed in accordance with the Institutional Animal Care and Use Committee (IACUC) guidelines set up by Tsinghua University. All animals were housed in isolated ventilated cages (maximal six mice per cage) barrier facility under conditions of a 12/12-hour light/dark cycle, 22-26 °C, 50%–60% humidity, and unrestricted access to sterile pellet food and water ad libitum in the Tsinghua University animal research facility, which is accredited by the Association for Assessment and Accreditation of Laboratory Animal Care International (AAALAC).

The previously described floxed Piezo1 (Piezo1$^{fl/fl}$) (Cahalan et al., 2015) and Piezo2 (Piezo2$^{fl/fl}$) (Ranade et al., 2014b) mice in C57BL/6 background were obtained from Dr. Ardem Patapoutian laboratory at the Scripps Research. Piezo1$^{fl/fl}$ and Piezo2$^{fl/fl}$ mice were crossed to obtain the double floxed P1/P2$^{fl/fl}$ mice. To delete both Piezo1 and Piezo2 in astrocytes, the P1/P2$^{fl/fl}$ mice were crossed with the hGFAP-Cre transgenic mice, which express the Cre recombinase under the control of the human glial fibrillary acidic protein (hGFAP) promoter (Zhuo et al., 2001). The resulting P1/P2$^{fl/fl}$ (defined as control, Ctrl) and hGFAP-Cre;P1/P2$^{fl/fl}$ (defined as conditional knockout, cKO) littermate mice were utilized for experiments. Piezo1$^{fl/fl}$ mice were crossed with the GFAP-Cre transgenic mice to generate the GFAP-Cre;Piezo1$^{fl/fl}$ (defined as Piezo1^{cKO}) mice.

To overexpress Piezo1 in astrocytes, our previously generated Piezo1-TG$^{fl\text{-}mCherry\text{-}stop\text{-}fl}$ mice (Zhang et al., 2019) were mated with the hGFAP-Cre mice to obtain the hGFAP-Cre;Piezo1-TG$^{fl\text{-}mCherry\text{-}stop\text{-}fl}$ mice, in which the loxP-franked mCherry sequence with a stop codon was excised, allowing the expression of the downstream eGFP-Piezo1 fusion protein. The resulting Piezo1-TG$^{fl\text{-}mCherry\text{-}stop\text{-}fl}$ (defined as Ctrl-TG) and hGFAP-Cre;Piezo1-TG$^{fl\text{-}mCherry\text{-}stop\text{-}fl}$ (defined as P1-TG) littermate mice were utilized for experiments.

The previously reported Piezo1-tdTomato knock-in mouse line (Piezo1-tdTomato-KI), in which the tdTomato coding sequence was knocked into the genetic sequence coding the C-terminus of the mouse Piezo1 protein (Ranade et al., 2014a), was purchased from the Jackson Laboratory. Homozygous mice were used for expression analysis.

Healthy mice were used in the experiments, and the age is specified in the text. In experiments involving adult neurogenesis and behavioral assays, we exclusively used male mice. No mice were used in previously unrelated experiments. Adult neural stem cells were isolated form 5-8 weeks old male WT mice, and the primary astrocytes were isolated from P0 male and female mice. The influence of sex was not evaluated in this study.

Cell lines

HEK293T cells obtained from Dr. Ardem Patapoutian laboratory were used for electrophysiology. Cells were cultured in Dulbecco's Modified Eagle Medium (DMEM) supplemented with 10% fetal bovine serum (FBS).

Primary mouse cell cultures

Cortical and hippocampal astrocytes were dissected from neonatal mice (within 24 hours after birth) and cultured in Dulbecco's Modified Eagle Medium (DMEM) (Gibco) supplemented with 10% fetal bovine serum (FBS) at 37 °C in a humidified incubator containing 5% CO_2.

Cortical and hippocampal neurons were acutely dissociated from neonatal mice (within 24 hours after birth) and cultured in Neurobasal™-A Medium and B-27 solution (GIBCO) at 37 °C in a humidified incubator containing 5% CO_2.

NSCs were isolated from the DG of 5-8 weeks old male mice and cultured in Neurobasal Medium containing 20 ng/mL basic fibroblast growth factor (FGF-2, K1606, PeproTech), 20 ng/mL epidermal growth factor (EGF, A2306, PeproTech), 1% N2 supplement (17502-048, GIBCO), 1% Antibiotic-Antimycotic, and 2 mM L-Glutamine at 37°C in a humidified incubator containing 5% CO_2.

METHOD DETAILS

RNA extraction and RT-PCR

The total RNA was extracted from primary mouse astrocytes and neurons using the RNA isolation kit (Axygen) according to the instruction manual. The related cDNAs were generated from the isolated RNA samples using the reverse-transcription kit (Bio-rad). Primers used for PCR of mouse astrocytes and neurons include

mPiezo1-Forward: ATCCTGCTGTATGGGCTGAC;
mPiezo1-Reverse: AAGGGTAGCGTGTGTGTTCC;
mGAPDH-Forward: CACAATTTCCATCCCAGACC;
mGAPDH-Reverse: GTGGGTGCAGCGAACTTTAT.

Primary culture of mouse astrocytes and neurons

Primary astrocytes were acutely dissociated according to the previously described method with some modifications (Schildge et al., 2013). Briefly, the cortical and hippocampal areas were dissected from neonatal mice (within 24 hours after birth), and dissociated in 0.25% trypsin-EDTA for 10 min and triturated in Dulbecco's Modified Eagle Medium (DMEM) (Gibco) supplemented with 10% fetal bovine serum (FBS) and plated into a culture flask (Corning) and incubated at 37 °C in the 5% CO_2 incubator. After 10 days of culture, the astrocytes were re-plated on coverslips, and used 6-24 hours later for measuring mechanically evoked cationic currents, Ca^{2+} influx and ATP release from astrocytes. Primary neurons were prepared as previously described (Chi et al., 2009). In brief, cortical and hippocampal neurons were acutely dissociated from neonatal mice (within 24 hours after birth) and treated with 0.25% trypsin for 7 min at 37 °C. Individual neurons were plated on glass coverslips incubated at 37 °C in a humidified incubator containing 5% CO_2. The medium was replaced 7 hours later with Neurobasal™-A Medium and B-27 solution (GIBCO). After 10 days of culture, the cultured neurons were used to measure mechanically evoked cationic currents.

Co-culture of primary mouse NSCs and astrocytes

NSCs were isolated from the DG of 5-8 weeks old male WT or genotype specified mice based on previously published methods (Guo et al., 2012). DGs were dissected from 400 μm coronal sections of forebrain under a microscope. After enzymatic digestion using MACS Neural Tissue Dissociation kit (130-092-628, MACS Miltenyi Biotec), 5 mL of Neurobasal Medium (21103-049, GIBCO) containing 10% FBS (10099-141, GIBCO), 2 mM L-glutamine (25030-081, GIBCO), and 1% Antibiotic-Antimycotic (15240-062, GIBCO) was added into each sample to stop digestion. After filtering through a 70-μm cell strainer (252350, BD Falcon) and washing with Neurobasal Medium containing 2 mM L-Glutamine and 1% Antibiotic-Antimycotic, the single-cell suspension was collected and cultured with Neurobasal Medium containing 20 ng/mL basic fibroblast growth factor (FGF-2, K1606, PeproTech), 20 ng/mL epidermal growth factor (EGF, A2306, PeproTech), 1% N2 supplement (17502-048, GIBCO), 1% Antibiotic-Antimycotic, and 2 mM L-Glutamine in a 5% CO_2 incubator at 37°C. Half of the medium was replaced every 2 days.

For co-culture experiments, NSCs were plated onto poly-L-lysine-coated glass coverslips in 24-well plates, and allowed to settle at 37°C in a 5% CO_2 incubator for 12 hours. For proliferation assay, transwell inserts (MCRP24H48, Millipore) containing astrocytes were transferred into 24-well plates containing NSCs. After 8 hours incubation, EdU (E10187, Invitrogen) was added into NSC culture medium for extra 4 hours followed by PFA fixation for immunostaining, imaging and quantification.

For the differentiation assay, 24 hours after plating, cells were changed into the differentiation medium, Neurobasal Medium containing 5 μM forskolin (F-6886, Sigma-Aldrich), 1 μM retinoic acid (R-2625, Sigma-Aldrich), combined with lentivirus as indicated for 4 days, then fixed with 4% paraformaldehyde (PFA) for 30 minutes, washed with PBS for 10 minutes, and subjected to immunocytochemistry analyses.

EdU labeling

For analysis of NSC proliferation in the adult DG, mice at 5 months were intraperitoneally injected with EdU (E10187, Invitrogen) 4 times at a dosage of 40 mg/kg body weight within 8 hours with 2 hours interval. Tissue processing and quantification of EdU+ cells within the SGZ and granule cell layer were carried out as previously described (Wang et al., 2019a). Slices were incubated in the EdU click reaction buffer for 30 minutes. After washing, the antibody staining steps were similar to the ones described for floating sections. The results were presented as the number of EdU^+ cells in a cubic millimeter of DG.

Transient transfection

Human Embryonic Kidney 293T (HEK293T) cells and primary astrocytes were grown in Dulbecco's Modified Eagle Medium (DMEM), 10% fetal bovine serum (FBS). HEK293T cells were plated in 24-well plates and transfected with 1 μg of P2X7 for serving as sniffer cells using Lipofectamine 3000 according to the manufacturer's instructions (Invitrogen). After cultured for 10 days, astrocytes were replated and transfected with 1 μg of Piezo1 and Piezo1-ΔEL15-16 using Lipofectamine 3000. 24-48 hours post transfection, cells were subjected to electrophysiology, single-cell Ca^{2+} imaging and co-culture with NSCs.

Immunohistochemistry

Histological analyses of mouse brains were performed as described previously with modifications(Wang et al., 2019a). Briefly, mice were euthanized, and then trans-cardiac perfused with saline. Tissues were dissected out, fixed overnight in 4% PFA, and then equilibrated in 30% sucrose. The floating coronal brain serial sections (40 μm in thickness) through the entire DG were maintained in order and stored in 96-well plates filled with cryoprotectant solution (glycerol, ethylene glycol and 0.1 M phosphate buffer, pH 7.4, 1:1:2 by volume) in a -20°C freezer. Tissue sections were blocked with TBS++ (TBS containing 3% donkey serum and 0.3% Triton X-100) for 1 hour at room temperature, and stained with the primary antibodies. The following primary antibodies were used: Nestin (Aves Labs, chicken, 1:500), Mcm2 (BD Biosciences, mouse, 1:500), DCX (Santa Cruz, goat, 1:500), Sox2 (Santa Cruz, goat, 1:500), GFAP (DAKO, rabbit, 1:1000), Tbr2 (Abcam, rabbit, 1:500), NeuN (Abcam, mouse; 1:500), GFP (Cell Signaling, rabbit, 1:500), Satb2 (Abcam, rabbit, 1:500), Ctip2 (Abcam, rabbit, 1:500), Cux1 (Proteintech, rabbit, 1:500), Foxp2 (Abcam, rabbit, 1:500) and RFP (Rockland, rabbit, 1:500).

For the combination of nestin and EdU staining, antigen retrieval was required. Antigen retrievals were performed in citrate buffer (pH 9.0) with a microwave for 10 minutes at 95°C followed by 20 minutes cool down at RT.

For multi-color immunostaining of mouse brain sections, mouse brain tissues were fixed in 4% paraformaldehyde for 24 hours and embedded in paraffin. Five-micrometer sections of tissues were placed on coated slides for immunohistochemical staining (IHC). After deparaffinization and rehydration, antigen retrievals were performed in citrate buffer (pH 6.0) with a microwave for 20 minutes at 95°C followed by 20 minutes cool down at RT. After the quenching of endogenous peroxidase in 3% H_2O_2, slides were incubated with blocking reagent (ZLI-9022, ZSGB-BIO) for 30 minutes at RT. Antigens were then successively detected using the manufacturer's protocol. Briefly, primary antibody was incubated for 2 hours at 37°C, followed by incubation of biotinylated secondary antibody. Then the HRP-conjugated streptavidin is added to the tissue sample and incubated for further 30 minutes (Polink-1 HRP polymer detection kit, GBI Labs) and detected by TSA-fluors (1:100, 20-60 seconds, NEL797001KT, PerkinElmer), after which the primary and secondary antibodies were thoroughly eliminated by heating the slides in citrate buffer (pH 6.0) for 10 minutes at 95°C using microwave. In a serial fashion, each antigen was labeled by distinct fluorophores. Slides were mounted in Prolong (Invitrogen) and visualized by laser scanning confocal microscopy LSM 880 microscope (Carl Zeiss AG).

Single-cell Fura-2 Ca^{2+} imaging

Primarily cultured astrocytes grown on coverslips were subjected to single-cell Yoda1 Ca^{2+} imaging as described previously (Geng et al., 2020). In brief, cells were washed with the Ca^{2+} imaging buffer (1 x HBSS with 1.3 mM Ca^{2+}, 10 mM HEPES, pH 7.2) and then loaded with the Ca^{2+} imaging buffer containing 2.5 μM Ca^{2+} indicator dye Fura-2 and 0.05% Pluronic F-127. 30 min after Fura-2 loading, cells were washed twice with the Ca^{2+} imaging buffer. The Fura-2 signals excited at either 340 nm or 380 nm were captured by an inverted Nikon-Tie microscope with a CCD camera and Lambda XL light box (Sutter Instrument). Intracellular Ca^{2+} concentration was indicated as 340/380 by using MetaFluor Fluorescence Ratio Imaging software (Molecular Device). 5 μM Yoda1 (Pharmacodia) dilated from a 30 mM stock solution in DMSO was used for activating Piezo1. For poking-induced Ca^{2+} responses in astrocytes, Fura-2 loaded cells were subjected to mechanically stimulation similar to that described above for electrophysiologic recording of mechanically poked cells.

Two-photon Ca^{2+} imaging of hippocampal slices and data analysis

The brain slice for astrocyte imaging were prepared as previously described (Rungta et al., 2016). In brief, 2 to 5 month-old male littermate mice were anesthetized with the inhalation anesthetic isoflurane, and then perfused with ice-cold oxygenated artificial cerebrospinal fluid (ACSF). Acute hippocampal slices (300 μm thick) were prepared using a VF-300 microtome (Precision Instruments) and maintained at room temperature and perfused with ACSF continuously bubbled with 95% O_2 and 5% CO_2. ACSF contained (in mM): 124 NaCl, 26 $NaHCO_3$, 3 KCl, 2 $CaCl_2$, 1.25 KH_2PO_4, 1 $MgSO_4$ and 10 glucose (Sigma) (pH = 7.4).

The slice in the oxygenated ACSF was incubated with the calcium indicator Fluo-4 AM (10 μM) for 1h at room temperature and then the astrocyte-specific dye SR101 (1 μM) for 15 minutes at 37°C. After washed for three times, the dye-loaded slice was placed on a heating pad to maintain a 37°C condition. Live imaging was performed with two-photon microscope in a frame-scan mode at depth below the surface ranging from 50 to 200 μm, using a 25 ×/1.05 NA water objective (XLPLN25XWMP2, Olympus) at typically 512 × 512 pixel resolutionan mode at depth below the surface ranging from 50 to 200 ologic recordi set at 825 nm. Baseline images were recorded for about 300s for detecting spontaneous Ca^{2+} transients. 500 μM ATP was then applied manually to assay the response of astrocytes in the brain slice.

The imaging data set across the entire time series was analyzed using the NIH ImageJ and Imaris 9.7 softwares. Motion artifacts were corrected using Image J with the TurboReg plugin. SR101 and Fluo-4 AM co-labeled astrocytes were selected as regions of

interests (ROIs) for analysis of spontaneous Ca^{2+} transients and ATP-induced Ca^{2+} responses. The mean fluorescence intensity of each ROI within the time series during either the baseline recording or ATP application was measured. The change of the Fluo-4 intensity was expressed as $\Delta F/F0$, where $\Delta F = Ft - F0$ and F0 and Ft represent the baseline fluorescence and the fluorescence signal at the given time, respectively. The percentage of cells showing spontaneous calcium transients was defined as the number of astrocytes displaying spontaneous Ca^{2+} transients divided by ATP-responsive cells. The frequency of Ca^{2+} transient was analyzed from cells showing spontaneous Ca^{2+} transients.

Western blotting

Cell lysates derived from primary astrocyte cells or dorsal root ganglia neurons were prepared using the RIPA buffer (Beyotime Biotechnology) with a cocktail of protease inhibitors (Roche) and were then subjected to SDS-PAGE gels and electrophoresis separation. The proteins were transferred to 0.45 μm PVDF membranes (Millipore) for western blotting according to the procedure described previously (Zhang et al., 2017). In brief, the membrane was blocked by 5% non-fat milk (Bio-Rad) in TBST buffer (TBS buffer with 0.1% Tween-20) and incubated with our previously generated Piezo1 and Piezo2 antibodies (1:1000) used (Wang et al., 2019b; Zhang et al., 2017) or β-actin antibody (CST, 1:3000) for overnight. After 3 times of washing with TBST buffer, the membrane was incubated with the peroxidase-conjugated anti-rabbit IgG secondary antibody (CST, 1:10,000) at room temperature for 1 hour, followed with washing and detection using the enhanced chemiluminescent (ECL) horseradish peroxidase (HRP) substrate (Pierce).

Immunofluorescent staining of primarily cultured astrocytes

Primary astrocytes derived from Piezo1-tdTomato-KI mice (Jackson lab) or WT mice were cultured on coverslips. Cells were subjected to fixation in 4% paraformaldehyde (PFA) for 30 min, permeabilization with 0.2% Triton X-100, blocking with 3% BSA for 1 hour at room temperature, incubation with primary antibodies [anti-DsRed antibody (1:1000; clontech) and anti-GFAP (1:1000; Jackson lab)] at 4 °C for overnight. After washed with PBST for three times, the cells were incubated with secondary antibodies [anti-chicken cy3 (1:1000; Jackson lab) and Alexa Fluor donkey anti-rabbit 488 (1:1000; life Technologies)] for 1 hour at room temperature. After washed with PBST for three times, nuclei were counterstained with DAPI (Life Technologies). The coverslips were dried and mounted with Prolong Gold antifade reagent (Thermo). Fluorescence images were acquired using the Nikon A1 confocal microscope with a 60× objective at the SLSTU-Nikon Biological Imaging Center.

ATP infusion

ATP was diluted in 0.9% saline to a concentration of 10 μM ATP or saline alone was infused into the hippocampus of 5-month-old mice using micro-osmotic pumps (flow rate 0.25 μL/hr, Model 1002D, ALZET) for 12 days. Micro-osmotic pumps filled up with ATP or saline alone were connected with cannulas and balanced in saline at 37°C for at least 6 hours. The cannulas were implanted stereotaxically in the hippocampus following coordinates: anteroposterior, −2 mm; lateral, +/−1.7 mm; ventral, −1.9 mm (from dura). After 6 or 12 days of infusion, the pumps were removed and mice were prepared for experiments.

Stereotaxic injections

All brain injections were performed with a stereotaxic apparatus (RWD) with a microdispensing pump (World Precision Instruments) holding a beveled glass needle with ~50 mm outer diameter. For injections into adult hippocampus, mice were anesthetized with avertin, head fixed with a stereotaxic frame, and treated with ophthalmic eye ointment. For sparsely labeling hippocampal neurons, 1μl of diluted AAV9-hSyn1-eGFP was injected at a rate of 1 μl/min into the hippocampus using coordinates: anteroposterior, −2 mm; lateral, +/−1.7 mm; ventral, −1.9 mm (from dura). A dilution of 1:1000 in sterile saline was used for experiments measuring dendritic spine density and single neuron morphology. For astrocyte labeling, 1μl of diluted lenti-GfaABC1d-EGFP was injected at a rate of 1 μl/min into the hippocampus using the same coordinates. A dilution of 1:100 in sterile saline was used for experiments measuring astrocytic process length and morphology. Mice were allowed to recover on a heat pad before being returned to their cage.

Behavioral studies

Mouse behaviors were carried out using 5 to 9 month-old male littermate mice by investigators blinded to their genotypes. For open-field test, mice were individually placed in the center of an open-field apparatus (L × W × H in cm, 50 × 50 × 40) and allowed to explore freely for a period of 10 min. The routes of mice were recorded by a video camera. The total distances and time spent in the center were calculated using the Ethovision XT software (Noldus).

For Morris water maze (MWM) test, a circular water tank (diameter of 120 cm) was filled with opaque water at 22°C and a circular platform (diameter of 15 cm) was submerged 1 cm below the surface of the water in the center of one of the four virtually divided quadrants. Distal cues were fixed on the wall of the tank as spatial map. Learning trials were carried out for 6-7 consecutive days, with 4 trials per session and 1 session per day. In every trial, mice were required to find the platform in 60 s and to remain on it for at least 10 s. Start locations were randomized. The value of each day was averaged from the 4 trials. A probe trial was performed 24 hour later after the last training. The platform was removed, and mice were allowed to return to the platform's previous position for 60 s. Mice were tracked using a video camera in both the learning trials and the probe trial. Collected data were analyzed using the Ethovision XT software (Noldus). The MWM test were repeated in three separate experiments.

For Y-maze test, each of the three enclosed arms was extended from the center of the maze. The mice were gently placed in the center and allowed to freely explore the three arms for a period of 6 min. Alternations were counted when a mouse entered each of the three arms in succession, in any order, without re-entering one of the arms. The route of mice was recorded by a video camera. The number of arm entries and the number of triads were recorded in order to calculate the percentage of alternation. Collected data were analyzed using the Ethovision XT software (Noldus). The Y-maze task were repeated in three separate experiments.

Field EPSP recordings of hippocampal slices

Electrophysiological recordings of hippocampal slices were performed as previously described(Chi et al., 2010). Hippocampal slices were prepared from 5 to 6 month-old male littermate mice according to the procedure as described in the above section of "two-photon Ca^{2+} imaging of hippocampal slices". Transverse hippocampal slices were incubated for at least 1 hour before transferred to the field excitatory postsynaptic potentials (EPSPs) recording chamber (MED-PG515A, Alpha MED Science), which was perfused with ACSF at a rate of 1.5 ml per minute at 33 °C for at least 20 min prior to the recording. The field EPSPs were recorded from CA3-CA1 synapses through the stimulation of the Schaffer collateral (SC) fibers using a stimulation intensity that elicited a 30% maximal response. The LTP was induced using the standard theta burst stimulation (TBS) (each contains 10 trains with four-pulse at 100 Hz bursts and 200 ms intervals and three sets of TBS separated by 20 s) and delivered at the same intensity as in the baseline recordings. Data acquisition and slope measurement were carried out using the multielectrode MED64 hardware and software packages (Panasonic). 4 μM GsMTx4 (Tocris Bioscience), 1 unit/mL Apyrase (NEB) and 3 μM ATP was prepared with ACSF immediately before use. The compounds were continuously perfused during the experiment. Control slices received ACSF alone.

Whole-cell electrophysiology and mechanical indentation stimulation

Patch-clamp experiments were performed using an Axopatch 200B amplifier (Axon Instruments) as previously described (Zhao et al., 2018). All experiments were performed at room temperature (22-25°C). In brief, primarily cultured astrocytes, NSCs or neuron were recorded using a standard tight seal whole-cell recording technique. The recording electrodes had a resistance of 2∼3 MΩ when filled with an internal solution containing (in mM): 133 CsCl, 10 HEPES, 5 EGTA, 4 MgATP, 1 $MgCl_2$, 1 $CaCl_2$ and 0.4 Na_2GTP (pH 7.3 with CsOH). The extracellular solution was containing (in mM): 133 NaCl, 10 HEPES, 10 glucose, 3 KCl, 2.5 $CaCl_2$ and 1 $MgCl_2$ (pH 7.3 with NaOH). Currents were sampled at 20 kHz and filtered at 2 kHz using the Clampex 10.4 software (Axon). Leak currents before mechanical stimulation were subtracted off-line from the current traces. Mechanical poking was delivered to the cell being patched under whole-cell configuration at an angle of 80° using a fire-polished glass pipette (the tip diameter 3∼4 μm) as previously described (Zhao et al., 2016). Downward movement of the probe toward the cell was driven by a Clampex controlled piezo-electric crystal micro-stage (Physik Instrument; E625 LVPZT Controller/Amplifier). The probe had a velocity of 1 μm ms^{-1} during the downward, upward motion and the stimulus was maintained for 150 ms. A series of mechanical steps in 1 μm increments was applied every 20 s. The membrane potential was held at -60 mV.

Measurement of ATP release from astrocytes

We adopted the previously developed "sniffer-cell" method (Hayashi et al., 2004) for detecting ATP released from cultured astrocytes. HEK293T cells were co-transfected with 2 μg of plasmid expressing the mouse P2X7 receptor and 0.2 μg of plasmid expressing EGFP using the Lipofectamine 3000 according to the manufacturer's instructions (Invitrogen). To measure the ATP dose-response of the P2X7-expressing HEK293T cells, the transfected cells were dissociated and plated on the coverslips. Different concentrations of ATP were puffed onto the recorded cells. On the day of sniffer cell recording, To measure ATP release from mechanically poked or Yoda1 treated astrocytes, transfected HEK293T cells were dissociated and plated on the coverslips on which primary astrocytes had grown. Whole-cell recording of EGFP-positive P2X7-expressing HEK293T cells was performed using an Axopatch 200B amplifier (Axon Instruments), while mechanically poking the neighboring astrocytes with a 6 μm-displacement lasting for 1 second or puffing Yoda1 to the neighboring astrocytes. The pipette solution contained (in mM): 140 KCl, 10 HEPES and 10 EGTA (pH7.4 with KOH). The extracellular solution contained (in mM): 150 NaCl, 10 HEPES, 10 glucose, 5 KCl, 2.5 $CaCl_2$, 1 $MgCl_2$ (pH7.4 with NaOH) at room temperature (22-25°C). The membrane potential was held at -70 mV. Currents were sampled at 20 kHz and filtered at 2 kHz using the Clampex 10.4 software (Axon).

We also detected the extracellular ATP level using a bioluminescent ATP assay kit according to the manufacture's instruction (Invitrogen detection technologies). Primary cultures of astrocytes were incubated in Hank's Balanced Salt Solution (HBSS) and shaken at 150 rpm for 30 min on an orbital shaker at 37°C in the CO_2 incubator. The supernatant was collected for the ATP assay, while the cells were lysed and protein concentrations were measured. A calibration curve was obtained from ATP standard solution. Luminescence was measured using a varioskan flash (Thermo Scientific, USA) according to the manufacturer's instructions. The ATP level was calculated from the standard curve and normalized to the total protein amount in each sample.

We also detected the extracellular ATP level using the newly developed GPCR activation-based $GRAB_{ATP}$ sensor (Wu et al., 2022) according to the manufacture's instruction (Vigene Biosciences, China). Primary cultures of astrocytes were cultured in 24-well plates as described above. 10 days after culture, astrocytes were infected with 1 μl pAAV2/9-GfaABC1D-ATP1.0 (10^{13} vg/ml) viruses for 2 weeks and then subjected to imaging. The Yoda1 (30 μM) and ATP (100 μM) induced changes of the ATP1.0 signal excited at 530 nm were captured by an inverted Nikon-Tie microscope with a CCD camera and Lambda XL light box (Sutter Instrument). The signal change was quantified by normalizing the amplitude of the peak response to the ($\triangle F/F_0$).

Cell-attached electrophysiology and stretch stimulation

For recording stretch-induced currents, primary astrocytes were recorded in the conventional cell-attached configuration. The intracellular solution contained (in mM): 130 NaCl, 10 HEPES, 10 TEA-Cl, 5 KCl, 1 $MgCl_2$ and 1 $CaCl_2$ (pH 7.3 with NaOH). The extracellular solution contained (in mM): 140 KCl, 10 glucose, 10 HEPES and 1 $MgCl_2$ (pH 7.3 with KOH). Currents were sampled at 20 kHz and filtered at 2 kHz using the Clampex 10.4 software (Axon). Membrane patches were stimulated with negative pressure pulses through the recording electrode using a Patchmaster controlled pressure clamp HSPC-1 device (ALA-scientific). Current was activated by pressure steps from 0 to -100 mm Hg (-10 mm Hg increments) for 500 ms. The membrane potential was held at -80 mV. The recording traces were averaged per cell for analysis.

QUANTIFICATION AND STATISTICAL ANALYSIS

Cell quantification

For quantification of cells expressing stage-specific markers, 1 in 12 serial sections starting at beginning of hippocampus (relative to bregma, −1.5 mm) to the end of hippocampus (relative to bregma, −3.5 mm) were used. Quantification of EdU+ cells and phenotypic quantification of EdU+ cells (double labeling with Nestin, Mcm2 or Tbr2) in the granule layer were performed using LSM880 confocal microscope (Zeiss) with ZEN software in at least 3 sections containing the dentate gyrus from at least 4 different animals. The value of n is described in figure legends.

Dendritic morphology analysis

For dendritic morphology analysis on 50-μm-thick floating brain sections, the AAV labeled neurons were imaged on a LSM 880 confocal microscope (Zeiss) with a 20× per objective. Z stacks of the dendrites of AAV labeled neurons were captured at 2-μm intervals, and analyzed by ImageJ software (NIH, Bethesda, Maryland, USA). Data were extracted for Sholl analysis and total dendritic length from each infected neuron. At least 20-30 cells per group from at least 3 different animals were analyzed. The value of n is described in the figure legends.

Dendritic spine quantification

Images were acquired with an LSM 880 Confocal Microscope with AiryScan (Zeiss) by using a 63x objective (NA 1.4) with 2x optical zoom. Z stacks were acquired at a step-size set at half the optical section. Images were taken in the molecular layer of the DG. Dendritic spine density was quantified using ImageJ by measuring a distance of at least 20 μm along a dendritic branch and then counting dendritic spines.

Data analysis

Data were analyzed with the Prism software (Graphpad prism for windows, version 6.0). Representative traces of currents were generated by Origin 7.0 (Origin Lab, Northampton, MA, USA). All data are shown as the mean ± SEM from at least three independent experiments. Data were analyzed statistically using the unpaired Student's t-test for two groups of data and the one-way ANOVA for multiple groups of data. The criterion for a significant difference was defined as $^{*}P < 0.05$, $^{**}P < 0.01$, $^{***}P < 0.001$ and $^{****}P < 0.0001$.